行政院原子能委員會
委託研究計畫研究報告

SOFC 電池堆結構耐久性研究與壽命評估(III)

Life Assessment and Structural Durability Analysis for SOFC Stacks (III)

計畫編號：992001INER047

受委託機關（構）：國立中央大學

計畫主持人：林志光 教授

核研所聯絡人員：江烈光、劉建國、吳思翰

聯絡電話：03-4267340

E-mail address：t330014@cc.ncu.edu.tw

報告日期：99.11

目錄

頁數

摘要

本研究目的在探討玻璃陶瓷和金屬連接板間的接合強度及破壞模式，所使用的玻璃陶瓷為核能研究所開發的一款代號為 GC-9 的材質，金屬連接板則是使用代號為 Crofer 22 H 和 APU 的商用肥粒鐵系不銹鋼。藉由製作兩款三明治試片，分別量測接合件在室溫與 800 ^{o}C 下的剪力及張力強度，並評估試片接合溫度、金屬連接板的預氧化處理、玻璃膠塗佈面的數量、時效處理、金屬連接板成分等因素對於接合件強度的影響。結果顯示，在 900 ^{o}C 下接合的試片，其張力強度和剪力強度皆高於在 850 ^{o}C 下接合的試片，乃是在較高的溫度下，玻璃陶瓷在金屬連接板上的潤濕性質會較好，二者的接合性也較佳。金屬連接板在 900 ^{o}C 下的預氧化處理並沒有助於接合強度的提升，且過多的預氧化處理反而會造成接合強度明顯的下降。雙層玻璃膠試片的接合強度高於單層玻璃膠的試片強度，乃是由於雙層玻璃膠試片的玻璃與金屬在接合過程中會有較好的潤濕效果。比起未時效試片而言，不同時效處理試片的接合強度值下降幅度為 17~19%。至於比較 Crofer 22 H 和 APU 二款金屬連接板試片的接合強度，可以發現 Crofer 22 H 試片提供較高的接合強度。由微結構及破斷面分析結果發現剪力接合試片有三種破壞模式。第一，脫層現象發生在玻璃陶瓷基材與鉻酸鋇層的界面，此破壞模式所對應的接合強度是最低的。第二，脫層現象發生於玻璃陶瓷基材與鉻酸鋇層的界面和破裂發生於玻璃陶瓷基材內部，具有中等的接合強度。第三，脫層現象發生於金屬連接板與氧化鉻層的界面和玻璃陶瓷基材與鉻酸鋇層的界面，此種破壞模式所對應的接合強度是最高的。至於張力接合件，破壞發生於玻璃陶瓷基材的內部會伴隨著較高的接合強度，破壞發生在玻璃陶瓷基材與鉻酸鋇層的界面和玻璃陶瓷基材內部則會伴隨著較低的接合強度。

Abstract

The objective of this study is to investigate the joint strength between a glass-ceramic sealant and metallic interconnect. The applied materials were the GC-9 glass ceramic developed at the Institute of Nuclear Energy Research (INER) and the commercial Crofer 22 H and APU ferritic stainless steels. A methodology of evaluating the joint strength at room temperature (RT) and 800 ^{o}C was developed by testing two types of sandwich-like specimens under shear and tensile loading. The effects of joining temperature, pre-oxidization of metallic interconnect, number of initial spreading side, aging treatment, and composition of metallic interconnect on the joint strength at RT and 800 ^{o}C were studied. The measured shear strength of the specimens joined at 900 ^{o}C was greater than that of those joined at 850 ^{o}C. Apparently, an increase of joining temperature could improve the joining performance due to a better wetting behavior of glass ceramic. A pre-oxidization treatment at 900 ^{o}C for 2 h did not generate a beneficial effect on the shear and tensile joint strength for all the given testing conditions. The joint strength of specimens with a double-layer of glass-ceramic sealant was greater than that of single-layer ones due to a better wetting behavior of the GC-9 glass-ceramic sealant in contact with the metal slice during joining. Compared to the shear strength at 800 ^{o}C for the unaged joint specimens, a 17-19% reduction of joint strength was observed for the aged ones with various aging times. In comparison of the shear joint strength between Crofer 22 H and APU specimens, it is found that an addition of Nb and W elements in the Crofer 22 H steel provides a greater bonding strength with the GC-9 glass-ceramic sealant. Through the analysis of interfacial microstructure, fracture modes of the joint were correlated with the measured strength. Three types of fracture modes were identified for the shear joint specimens. Firstly, the lowest joint strength was accompanied by delamination at the interface between the glass-ceramic substrate and an adjacent oxide layer, chromate ($BaCrO_4$). Secondly, fracture at the interface between the GC-9 glass-ceramic sealant and the chromate layer as well as in the GC-9 layer accompanied a medium joint strength. Thirdly, a high level of joint strength was accompanied by delamination at the interface between the metal substrate and the Cr_2O_3 layer as well as at the interface between the GC-9 substrate and $BaCrO_4$ layer. For the tensile joint specimens, a greater joint strength accompanied fracture in the glass-ceramic layer. However, delamination at the interface between the GC-9 substrate and $BaCrO_4$ layer was also involved in the fracture in addition to the fracture of the glass-ceramic layer, for a lower level of tensile joint strength.

1. INTRODUCTION

1.1 Solid Oxide Fuel Cell

Solid oxide fuel cells (SOFCs) are the most efficient devices invented for conversion of chemical fuels into electrical power. Compared with other fuel cells, the most important features of the SOFC are that (1) the utilization of solid oxides as the electrolyte which can prevent leakage or evaporation and (2) the operating temperature is higher. Solid oxides possess sufficiently high ionic conductivity at elevated temperature so that SOFCs must operate at the temperature range of 800-1000 ^{o}C. Without the application of noble catalysts, SOFCs can still proceed with electrochemical reactions. Through internal reforming, hydrocarbon fuels such as natural gas can be catalytically converted to hydrogen and carbon monoxide for direct use in SOFCs.

Figure 1 shows the operating principle of an SOFC using hydrogen as fuel [1]. The electrochemical reactions involved are shown below:

Anode: $H_2 + O^{2-} \rightarrow H_2O + 2e^-$ (1)

Cathode: $\frac{1}{2}O_2 + 2e^- \rightarrow O^{2-}$ (2)

Overall: $H_2 + \frac{1}{2}O_2 \rightarrow H_2O$ (3)

Fuel such as hydrogen is fed into the anode side where it is oxidized by reacting with oxygen ions to produce water and release electrons to the external electrical circuit. Oxidant flows through the cathode side such that oxygen is transformed into oxygen ions as a result of receiving electrons from the external circuit. By means of the thrust of differences in potential and concentration, oxygen ions migrate to the anode through oxygen vacancies in the electrolyte. The electrolyte conducts these ions between the electrodes by maintaining the overall electrical charge balance. Finally, the flow of electrons in the external circuit generates the electrical power, providing for electrical appliance.

There are two major configuration designs for SOFC developed, namely tubular and planar cells. The planar type is expected to be cost effective and mechanically robust and offer high surface, volumetric and gravimetric power densities [2]. For a unit cell, it consists of anode, cathode and electrolyte to perform a complete electrochemical reaction. In practical applications, a positive electrode-electrolyte-negative electrode (PEN) plate is fabricated by sintering anode, electrolyte and cathode together at high temperature. The PEN is also

called membrane electrode assembly (MEA). The power capacity of a single cell is limited. In order to obtain a higher voltage and power, interconnects which have high electrical conductivity and gas-separation ability are used to provide electrical conduction for several PEN plates in a serial connection. Structural scheme of a planar SOFC stack is shown in Fig. 2 [3]. Between the interconnect and PEN plate, a nickel mesh is inserted to work as both current connectors and fuel gas manifolds. In addition, high temperature hermetic sealants are needed and play an important role in planar SOFCs to prevent fuel and oxidant from mixing and leakage during operation.

1.2 Joint of Glass-Ceramic Sealant and Metallic Interconnect

Sealing designs developed for SOFC include rigid seals and compressive seals. In the type of compressive sealing such as mica-based sealants, the major advantage is that these seals are not rigidly fixed to other SOFC components. Using compressive seals, matching CTE with other adjacent components such as the electrode and interconnect is not as important as that in using rigid seals. However, maintenance of gas-tight compressive sealing requires an application of constant load during operation. On the other hand, rigid seals, such as brazing, glass and glass-ceramic sealants, do not require such a mechanical load, but have more strict requirements for good adherence and CTE match to prevent leakage and cracking [4]. Glass sealants are used in planar SOFC stacks because of easy fabrication and usage. During thermal cycles, considerable thermal stresses can be generated due to temperature gradients and thermal expansion mismatch. Glass sealants become brittle after melting and cooling such that they are very sensitive to cracking under tensile stresses [5]. To overcome the drawback of glasses, glass ceramics are fabricated by means of heat treatment to change the microstructure of glasses from an amorphous phase to crystalline phases. Therefore, glass ceramics have better mechanical properties and higher viscosity than glasses to withstand thermal stresses.

When a rigid type of sealing is applied to intermediate-temperature SOFC (IT-SOFC), joining the glass ceramic sealant with metallic interconnect is very common. Figure 3 [5] shows the locations where seals are used in a planar SOFC stack with metallic internal gas manifolds and metallic interconnects. Common seals include: (a) cell to metal frame; (b) metal frame to metal interconnect; (c) frame/interconnect pair to electrically insulating spacer; (d) stack to base manifold plate [5]. Seals (b) and (d) can be referred to as a joint

of glass-ceramic sealant and metallic interconnect.

During cyclic operation of SOFC, generation of thermal stresses is inevitable leading the seals to be subjected to tensile and shear stresses [6-8]. Once the stresses exceed the corresponding strength of the joint, the seals may fail leading to degradation of cell performance. For this reason, it is necessary to investigate the mechanical properties of the joint of glass-ceramic sealant and metallic interconnect for assessment of the structural reliability of an SOFC stack. The mechanical properties of a joint do not belong to that of a single material while they are interfacial properties between two materials. Any interaction between glass ceramic and metal may influence the mechanical properties of the joint. Unfortunately, these interactions such as undesirable chromate formation [9] and electrical short-circuiting [10] are difficult to avoid if ferritic chromia-forming alloys are applied as the interconnect. There is little work in the literature related to the mechanical properties of such a joint in SOFC. Only a few studies [2,11-14] have studied this subject which is important to advance the development of SOFC technologies.

In the study of Malzbender et al. [2], a symmetric shear test was developed to characterize the shear strength of the joint between a glass-ceramic sealant (BCAS, BaO-CaO-Al_2O_3-SiO_2) and a metallic interconnect (Crofer 22 APU) at the SOFC operating temperature (OT). In addition to shear strength, shear modulus and viscosity of the joint were also determined by a rheological model [2]. At the OT, the as-joined specimens exhibited viscous shear deformation while the viscous shear deformation became more difficult for additionally crystallized specimens [2]. Smeacetto et al. [11] evaluated the tensile joint strength between a glass ceramic (SACN, SiO_2-Al_2O_3-CaO-Na_2O) and a metallic interconnect (Crofer 22 APU) at room temperature (RT). Examination of the fractured samples revealed that fracture always occurred in the glass ceramic and never at the interface of the joint. In the study of Stephens et al. [12], the interfacial strength between the G18 glass ceramic and Crofer 22 APU substrate was tested at temperatures ranging from 25 to 800 ^{o}C under both tensile and shear loading. However, examination of the fracture surfaces revealed two different failure modes in the tensile tests: glass bulk failure mode referring to failure occurring through the glass layer, and interfacial failure mode referring to failure occurring at the glass-metal interface.

Chou et al. [9] investigated the tensile joint strength of a novel high-temperature sealing glass (SrO-CaO-Y_2O_3-B_2O_3-SiO_2) with a metallic interconnect (Crofer 22 APU) at RT. The bonding/wetting behavior of glasses to metals is intensely dependent on the nature of the surface of the metal. The

testing samples were pre-oxidized to generate oxide layers to simulate long-term exposure conditions. Effects of environmental aging, including oxidizing and reducing, were also studied. In a further study of Chou et al. [13], effect of aluminization of the metallic interconnect on the tensile strength of the joint at RT was studied. Three different processes for aluminization were evaluated. The results of that study [13] showed that aluminization could reduce undesirable chromate formation between alkaline earth silicate sealing glass and chromia-forming alloys.

As described in Ref. [11], in order to make a good adhesion between AISI 430 and a glass-ceramic sealant, a pre-oxidation heat treatment was essential. For the case of as-received AISI 430 without pre-oxidation treatment, the glass-ceramic sealant was more easily detached from the metallic interconnect. In the study of Donald [14], an appropriate metal oxide layer was generated by pre-oxidization of a metal substrate before sealing process. During sealing process, the oxide layer dissolved into the glass, and the interface between the glass and metal became saturated such that favorable bonding conditions would then prevail over the interface [14]. However, if sealing is attempted to a clean metal surface, a suitable redox reaction between the glass and metal is needed to achieve conditions suitable for chemical bonding [14]. It indicates that a pre-oxidization layer can provide the favorable bonding conditions with no need of a suitable redox reaction before the sealing process. In the study of Smeacetto et al. [15], a new glass was designed and used to join YSZ to Crofer 22 APU. Aging treatment in air caused a Cr-diffusion from Crofer 22 APU alloy to the glass-ceramic sealant only when the alloy was in the as-received condition, whereas the pre-oxidized specimens did not exhibit migration of Cr through the glass-ceramic sealant.

1.3 Purposes and Scope

The high OT enables SOFCs to obtain a superior efficiency of energy conversion while accompanying concerns such as degradation of materials which results from undesirable reactions between components. Structural durability of SOFC is affected by the thermal stress caused by considerable CTE mismatch between components and thermal gradient. Excessive thermal stresses may lead to fracture of components endangering the mechanical integrity of an SOFC stack. As hermetic sealants are weaker than other components of the stack, a systematic investigation of mechanical properties of joints between the glass-ceramic sealant and metallic interconnect at RT and OT

is essential for development of a reliable SOFC stack.

The objective of this study is to investigate the seal strength of a glass-ceramic sealant with a metallic interconnect. Two loading modes, tensile and shear forces, are applied to characterize the mechanical properties of the joint at both RT and 800 ^{o}C. Effects of joining temperature, pre-oxidation, and number of initial spreading side on the bonding strength of the joint are evaluated. In addition, some samples are also tested after aging at 800 ^{o}C in air to simulate the SOFC working environment. Fractographic and microstructural analyses are conducted with scanning electron microscopy (SEM) and correlated with the mechanical testing results. Results of the current study hopefully will provide useful information for prediction of the long-term structural reliability and development of planar SOFC.

2. MATERIALS AND EXPERIMENTAL PROCEDURES

2.1 Materials and Specimen Preparation

As mentioned in Section 1.2, for a planar SOFC stack with rigid sealing, glass- ceramic sealants are applied to bond each layer together and prevent leakage of air and fuel. Among the four sealing locations shown in Fig. 3, sealants used to seal a metallic frame to a metallic interconnect (S2) and a stack to a base manifold plate (S4) are classified into a joint of glass-ceramic sealant and metallic interconnect. In order to simulate the conditions of the joint subjected to thermal stresses at RT and OT, two types of sandwich-like specimens (metal/sealant/metal) were designed in this study for determining the mechanical properties of the joint and investigating the interfacial reactions.

In order to investigate the effect of chemical composition of the metallic interconnect on the joint strength, the two kinds of metal are used in this study. The metallic parts of the joint specimens are made of two commercial ferritic stainless steels, Crofer 22 H and Crofer 22 APU (ThyssenKrupp VDM GmbH, Werdohl, Germany), which are heat-resistant alloys especially developed for application in SOFCs. Chemical compositions of these two alloys are listed in Tables 1 and 2, respectively. Tables 3 and 4 [16] show the mechanical properties of Crofer 22 H and APU alloy. For both Crofer 22 H and APU, the yield strength, ultimate tensile strength, and Young's modulus were decreased but the elongation was increased with an increase in temperature. The glass ceramic used to join the two metal slices was developed at the Institute of

Nuclear Energy Research (INER). The major composition of the glass-ceramic sealant includes SiO_2, B_2O_3, Al_2O_3, and BaO. The glass ceramic, designated as GC-9, was prepared firstly by melting appropriate amounts of reagents in a powder mixture. The powder mixture was heated to 1550 ^oC and held for 10 h to form the glass paste. The glass paste was then poured into a mold and annealed in a furnace at 680 ^oC for 8 h to produce the glass ingot. Finally, the glass ingot was cooled down to RT and ball-milled to produce the glass powder. An important factor for selection of suitable glass sealants is the glass transition temperature (T_g), because the key mechanism of the glass sealant at operating condition is viscosity [3]. The thermal properties, such as T_g, softening temperature (T_s), crystallization temperature (T_c), and CTE, were measured by a differential scanning calorimetry (DSC) and a dilatometer at INER [17]. The T_g, T_s, T_{c1}, and T_{c2} of the non-aged GC-9 bulk glass are 668 ^oC, 745 ^oC, 820 ^oC, and 864 ^oC, respectively [17]. Figure 4 [18] shows the thermal expansion curves of the non-aged and aged GC-9 bulk glass. After aging treatment, the T_g and T_s of the GC-9 bulk glass were changed to 650 ^oC and 826 ^oC, respectively. Table 5 [19] shows the flexural strength and Young's modulus for the non-aged, sintered GC-9 glass at various temperatures.

Figure 5 shows the scheme of two types of joint specimens for tensile test (Fig. 5(a)) and shear test (Fig. 5(b)), respectively. The as-received metal plates were cut into slices in the dimensions of 95 mm x 25 mm x 2.5 mm. A pin hole was drilled in each steel slice for applying pin loading. In order to minimize bending and twisting during test, the force was applied by means of pin loading. For shear specimens, an edge of each steel slice was milled from the original thickness of 2.5 mm to 1 mm with an area of about 8 mm x 25 mm. After machining of the steel slices, GC-9 glass slurry was spread on the joining region of each steel slice to make a half-specimen. The nominal joining areas were 25 mm x 2.5 mm and 25 mm x 5 mm for tensile and shear specimens, respectively. The glass slurry was made of a mixture of glass powder dispersed in ethanol. The half-specimen was then put in a furnace at 70 ^oC to dry the slurry. A joint specimen was assembled by placing a half-specimen onto another steel slice to form a steel/glass ceramic/steel sandwich specimen through appropriate heat treatments. In addition, for studying the effect of number of spreading side on the joint strength, a half-specimen was placed on another half-specimen to form a sandwich specimen through the same joining heat treatments.

Based on the assembling procedures for a practical planar SOFC stack developed at INER, the joint specimens were firstly heated to 350 ^{o}C and 750 ^{o}C and held for 1 h each to completely remove the ethanol in the glass slurry. After that, the specimens were held at 850 ^{o}C for 4 h to let the GC-9 glass react with the metallic slices and join together. In order to evaluate the effect of joining temperature on bonding strength, another assembling process was carried out. Some specimens were firstly held at 500 ^{o}C for 1 h and heated to 900 ^{o}C with a hold time of 4 h. The heating rate at each heating step in the given assembling processes is 5 ^{o}C/min. For investigating the effect of oxide layer on the joining quality, some steel slices were pre-oxidized at 900 ^{o}C for 2 h and 20 h before the assembling treatment. To study the effect of aging treatment on the joint strength, some as-sealed specimens were aged in air at 800 ^{o}C for 250, 500, and 1000 h.

2.2 Mechanical Testing

For determination of mechanical properties of the joint at RT and 800 ^{o}C, the specimens were tested under uni-axial loading on a commercial closed-loop servo-hydraulic test machine (MTS 810). In order to minimize bending and twisting during test, pin loading was applied in the tests. For the high-temperature tests, the specimens were heated to 800 ^{o}C with a rate of 5 ^{o}C/min and held for 15 min to reach thermal equilibrium before mechanical testing. The mechanical tests were conducted by means of displacement control with a loading rate of 0.5 mm/min. For each case, about 5-7 specimens were repeatedly tested and the average strength was determined.

2.3 Microstructural Analysis

After mechanical testing, fracture surface of each specimen was examined with an optical microscope to determine the true joining area. In order to investigate the characteristics of interfaces in the joint, some samples were cut along the longitudinal direction to observe the cross sections. The cross sections of the samples were finely polished to optical finish. SEM was also used to examine the interfacial morphology between the glass-ceramic sealant and metallic interconnect. The energy dispersive spectrometer (EDS) module was used for composition analysis in order to understand the elemental distribution in the glass-ceramic sealant and metallic interconnect. The fracture behavior and mode of the joint under tensile stress and shear stress were

also characterized.

3. RESULTS AND DISCUSSION

Glass-ceramic sealants suffer thermal stresses of tensile and shear modes during operation as a result of CTE mismatch between glass-ceramic sealants and other components in a planar SOFC stack [6]. Unfortunately, the thermal stresses caused by CTE mismatch are inevitable because the glass-ceramic sealants are rigidly bonded with adjacent components. If the critical stresses in the sealants are too large, the glass-ceramic sealants may fail due to fracture of bulk material or interfacial delamination between the joining surfaces. In order to avoid these problems, there are two approaches: (a) improvement of the mechanical properties of glass-ceramic sealants; (b) enhancement of interfacial bonding strength between the glass-ceramic sealants and metallic interconnects.

In the present work, suitability of the GC-9 glass ceramic for use in planar SOFC was investigated. Sandwich-like (metal/GC-9/metal) specimens were used to determine the tensile and shear joint strength at RT and 800 ^{o}C. Formation of adhesive oxide layers is the main mechanism of interfacial joining between the glass ceramic and metallic interconnect. The bonding strength of the joint originates from the mutual Van Der Waals force of the formed oxide layers. The high-temperature joining mechanism of the GC-9 glass ceramic and Crofer 22 APU alloy involves formation of two oxide layers with a Cr_2O_3 layer on the surface of Crofer 22 APU connected with a $BaCrO_4$ layer on the surface of GC-9 [20].

In the following discussion, some of the results have been reported in the thesis of Tian [21], who worked together with the author on the current subject. The present work is an extension study of the previous work of Tian [21], as more specimens were tested to get more data for a comprehensive study of the investigated issues.

3.1 Effect of Joining Temperature on the Joint Strength

During the joining process, the bonding characteristic of the joint was controlled by the joining temperature. It is important to understand the effect of joining temperature on the joint strength. Sandwich-like (Crofer 22 H/GC-9/Crofer 22 H) specimens were joined at 850 ^{o}C (hereafter called HT850S) and 900 ^{o}C (HT900S), respectively, for comparison. Details of the

procedures in the two heat treatments were described in Section 2.1. After joining treatment, the specimens were tested under shear loading at RT and 800 ^{o}C, respectively. The typical force-displacement curves for all the shear specimens tested at RT and 800 ^{o}C are shown in Fig. 6. The force-displacement curve at RT exhibited a typical pattern of brittle fracture. However, the force-displacement curve at 800 ^{o}C exhibited a non-linear failure mode. As the testing temperature of 800 ^{o}C is higher than the T_s (745 ^{o}C) of the GC-9 glass ceramic, the failure behavior at 800 ^{o}C became a ductile mode. Note that the final displacement at 800 ^{o}C was greater than that at RT and the testing time at 800 ^{o}C was longer than that at RT under the same loading rate. These are evidences for the softening behavior of the glass ceramic at 800 ^{o}C.

Figure 7 shows the shear strength at RT and 800 ^{o}C for the joint specimens with two different joining temperatures. In Fig. 7, the height of a solid bar indicates the average strength value and the ends of an error bar represent the maximum and minimum strength values for each given condition. For the HT850S specimens, the average shear strength was 3.6 MPa at RT and 4.3 MPa at 800 ^{o}C. For the HT900S specimens, the average shear strength at RT was 4.9 MPa and decreased to 4.4 MPa at 800 ^{o}C. The shear strength of HT900S was greater than that of HT850S at RT and both were comparable at 800 ^{o}C. This result indicates that an increase of joining temperature from 850 ^{o}C to 900 ^{o}C could improve the wetting behavior of the GC-9 glass ceramic on the surface of the Crofer 22 H and further enhance the joining performance between the two materials.

Figure 8 shows the failure patterns in the HT850S shear specimens tested at RT and 800 ^{o}C. There are two Crofer 22 H substrates in Fig. 8(a) [21]; the lower one was separated from the glass ceramic after testing and the upper one was still adhered with the GC-9 glass ceramic (yellow region). As shown in Fig. 8(a) [21], the shape of the peeled Cr_2O_3 layer is comparable with that of the region left on the other metal substrate. There is a shining region in the middle of the lower Crofer 22 H substrate, and there is a darker region in the upper half on the surface of the GC-9 with a similar shape to the shining region. The darker region is a chromia layer peeled from the metal substrate. Hence, a metallic luster of the metal substrate appears in the shining region. However, this phenomenon was not observed in Fig. 8(b). There is no obviously shining region on the lower Crofer 22 H slice in Fig. 8(b), but still a slightly bright region was observed on the surface of the Crofer 22 H slice. The composition of the slightly bright region was identified as a chromate ($BaCrO_4$). Note that the chromate also appears in the peripheral of the shining region in Fig. 8(a) [21].

Based on these two failure patterns, it can be concluded that, for HT850S shear specimens, there are two fracture modes which depend on testing temperature. Firstly, for the specimens tested at RT, delamination occurred at the interfaces between the glass-ceramic substrate and chromate or between the metal substrate and chromia. Secondly, for the specimens tested at 800 ^{o}C, delamination always occurred at the interface between the glass-ceramic substrate and chromate because the glass-ceramic substrate is softer at 800 ^{o}C. In other words, the glass-ceramic substrate was not tightly bonded with its oxide layer at 800 ^{o}C.

The typical fracture patterns in the HT900S shear specimens tested at RT and 800 ^{o}C are shown in Fig. 9. For the specimens tested at RT (Fig. 9(a)), it can be seen that in addition to delamination at interfaces, fracture even took place in the glass-ceramic substrate. A similar phenomenon was observed in the specimens tested at 800 ^{o}C (Fig. 9(b)). These results suggest that the interfacial bonding performance of HT900S is better than that of HT850S, so the shear strength of HT900S is greater than that of HT850S, as shown in Fig. 7.

Figure 10 shows the optical and SEM micrographs of a region of fracture surface without adhered glass ceramic. There are three distinct zones with various colors in the observed region, as shown in Fig. 10(a). As shown in Fig. 10(b), the three zones are the metal substrate, chromate ($BaCrO_4$) layer and chromia oxide layer of Crofer 22 H. High magnification views of the three zones are shown in Fig. 11. A smooth surface was observed at the zone of metal substrate, as shown in Fig. 11(a). In Fig. 11(b), the peeled $BaCrO_4$ from the surface of the glass-ceramic sealant is observed. A crystal structure is visible at the zone of the oxide layer of Crofer 22 H, as shown in Fig. 11(c). Such crystals are the spinels at the top of chromia. By means of EDS analysis, element distributions in these three zones are confirmed and shown in Fig. 12. As shown in Fig. 12(b), a high intensity of Fe was found in the region of metal substrate. The distributions of Cr, Mn and O shown in Figs. 12(c), (d) and (e), agree with the corresponding layers. The shape of the region of a high intensity of Ba agrees with that of the corresponding region supposed to be the $BaCrO_4$ and it is confirmed that this region in Fig. 11(b) is indeed the peeled chromate. These results indicate that the fracture mode indeed involves delamination of the interface of glass-ceramic substrate/chromate or metal substrate/chromia.

3.2 Effect of Pre-Oxidization on the Joint Strength

A pre-oxidization layer on metal is favorable for bonding a glass and metal as the oxide layer during sealing process can dissolve into the glass to make the interface between the glass and metal become saturated [14]. As described in Ref. [11], in order to obtain a good adhesion between AISI430 steel and SACN glass ceramic, a pre-oxidation heat treatment was essential. However, the results in Ref. [9] indicated that the joint strength of a SrO-CaO-Y_2O_3-B_2O_3-SiO_2 glass with Crofer 22 APU at RT was degraded if the thickness of oxide scale was greater than 1-2 μm while oxide scales thinner than 0.5 μm had no effect on joint strength. In other words, the pre-oxidation treatment had no positive effect on the joint strength between a glass sealant and metallic interconnect. The results in Ref. [9] exhibited an opposite trend to that of the pre-oxidation heat treatment results in Ref. [11]. Accordingly, further research is needed to investigate the pre-oxidation effect on the joint strength. In order to study the effect of pre-oxidation heat treatment, the Crofer 22 H alloy was pre-oxidized to different extents and then joined with the GC-9 glass ceramic in the current study.

For the shear joint specimens, POHT850S and POHT900S, used to investigate the effect of pre-oxidized metallic interconnect on the joint strength, the Crofer 22 H substrates were heat-treated in air at 900 ^{o}C for 2 h to form an oxide layer on the metal surface before joining. For the tensile joint specimens, POHT900D and LPOHT900D, used to investigate the effect of pre-oxidation treatment time on the joint strength, the Crofer 22 H substrates were heat-treated in air at 900 ^{o}C for 2 and 20 h, respectively. After pre-oxidization heat treatment, the joining processes were then performed as described in Section 2.1. Figure 13 shows the shear strength of pre-oxidized joint specimens tested at RT and 800 ^{o}C for the two specified joining temperatures. For the pre-oxidized POHT850S specimens, the average shear strength at RT was 1.6 MPa but increased to 2.4 MPa at 800 ^{o}C. For the pre-oxidized POHT900S specimens, the average shear strength at RT was 5.6 MPa and decreased to 4.2 MPa at 800 ^{o}C. Similar to the results of the specimens without pre-oxidization treatment described in Section 3.1, the shear strength of POHT900S was greater than that of POHT850S at both RT and 800 ^{o}C. These results once again confirm that a joining temperature of 900 ^{o}C is better than that of 850 ^{o}C in terms of joint strength.

In comparison of the shear strength between HT850S and POHT850S specimens, it is seen that the shear strength was significantly degraded by the pre-oxidization treatment, as shown in Fig. 14. As for the HT900S and POHT900S specimens joined at 900 ^{o}C, a pre-oxidization treatment slightly

degraded the shear joint strength at 800 ^{o}C but improved a little bit the shear joint strength at RT (Fig. 15). These results indicate that the pre-oxidization of Crofer 22 H indeed affected the joining performance and the influence was dependent on the joining temperature which also affects the wetting behavior of the glass ceramic on the metal surface. Based on the comparisons given in Figs. 14 and 15, a pre-oxidization treatment at 900 ^{o}C for 2 h did not significantly improve the shear strength of the GC-9/Crofer 22 H joint specimen indicating a different trend from that in Ref. [11] but a similar one to that in Ref. [9].

The tensile strength results of pre-oxidized joint specimens tested at 800 ^{o}C is shown in Fig. 16. The average tensile strength of the as-received HT900D specimens was 12.7 MPa and comparable with that (12.6 MPa) of the 2-h pre-oxidized POHT900D specimens. However, for the long-term (20 h) pre-oxidized LPOHT900D, the average tensile strength was 7 MPa. The tensile strength of the joint specimens with the a 20-h pre-oxidized treatment was considerably degraded indicating that a long-term pre-oxidization treatment of the Crofer 22 H slices deteriorated the bonding performance between the GC-9 glass ceramic and Crofer 22 H alloy. In addition, a short-term (2 h) pre-oxidized treatment did not generate noticeable enhancement or degradation on the tensile joint strength. Both the shear and tensile joint strength results shown in Figs. 14-16 clearly indicate that neither a 2-h nor a 20-h pre-oxidization treatment of the given metallic interconnect would effectively improve the bonding strength between the given glass-ceramic sealant and metallic interconnect. Although Ref. [11] reported that a pre-oxidization treatment could improve the bonding performance between silicate glasses with metallic interconnects, the conclusions were made based on microstructural observations without mechanical testing of joint strength.

Typical fracture patterns of the pre-oxidized shear specimens of POHT850S tested at RT and 800 ^{o}C are shown in Fig. 17. The fracture patterns shown in Figs. 17(a) and 17(b) are comparable, as delamination all occurred at the interface between the glass-ceramic substrate and chromate. As compared to Fig. 8, it indicates that the pre-oxidization of Crofer 22 H indeed has no positive effect on the joint strength of HT850S specimens. For the pre-oxidized shear specimens of POHT900S, the representative failure patterns at both RT and 800 ^{o}C are shown in Fig. 18 and are comparable with those in the as-received ones (Fig. 9). This might explain why the shear strength of the joint specimens joined at 900 ^{o}C was not significantly enhanced by the given pre-oxidization treatment. Typical fracture patterns of the pre-oxidized tensile specimens

tested at 800 ^{o}C are shown in Fig. 19. For the tensile specimens without pre-oxidization (HT900D), fracture all took place in the glass-ceramic substrate, as shown in Fig. 19(a). This implies that the bonding strength at interface was larger than that of the glass-ceramic substrate. For the 2-h pre-oxidized tensile specimens (POHT900D), most of the fracture also occurred in the glass-ceramic substrate, while delamination was occasionally observed at the interface, as shown in Fig. 19(b). However, for the 20-h pre-oxidized tensile specimens (LPOHT900D), extensive delamination was observed on the fracture surface, as shown in Fig. 19(c). It indicates that the long-term pre-oxidization treatment of Crofer 22 H has negative effects on the joint strength of HT900D tensile specimens.

Figure 20 shows the SEM micrograph of a cross-sectional view of the interface between the GC-9 and Crofer 22 H in an HT900D joint specimen without pre-oxidization. Two distinct zones can be observed; the upper zone in the figure represents the glass-ceramic sealant, while the lower region is the Crofer 22 H. A good adhesion between the glass-ceramic sealant and Crofer 22 H can be observed. A continuous and crack-free interface is present indicating a good physical compatibility between the two materials. The chromia oxide (Cr_2O_3) layer on the metal side of HT900D is not obvious. SEM micrographs of a cross-section of the interface in POHT900D are shown in Fig. 21. For the 2-h pre-oxidized POHT900D specimen, a good adhesion also can be observed. A bright and non-uniform chromia oxide layer on the metal side is clearly seen at the interface, as shown in Fig. 21(a). As shown in Fig. 21(b), the thickness of chromia oxide layer in POHT900D is about 0.3 μm. Figure 22 shows the SEM micrographs of a cross-section of the interface between the GC-9 and Crofer 22 H in a LPOHT900D specimen with 20-h pre-oxidization. As shown in Fig. 22, a good adhesion between the glass-ceramic sealant and Crofer 22 H is also observed. As compared to Figs. 20 and 21, the chromia oxide layer in LPOHT900D is more uniform. The thickness of chromia oxide layer in LPOHT900D can be clearly measured and is about 1.1 μm, as shown in Fig. 22(b). In corresponding to the mechanical testing results in Fig. 16, the above microstructural observations clearly indicate that the joint strength is significantly degraded if the thickness of chromia oxide layer is greater than 1.1 μm. Such a trend was also reported in Ref. [9]. In this regard, although a qualitatively good adhesion between the glass-ceramic sealant and metallic interconnect could still be seen in a long-term pre-oxidized joint specimen, the long-term pre-oxidization heat treatment would not generate any beneficial effect on the joint strength according to the mechanical testing and

microstructural analysis results present in the current work.

3.3 Effect of Pre-Oxidization on the Joint Strength

In Sections 3.1 and 3.2, HT900S and POHT900S specimens with a single glass-ceramic layer were joined by placing a Crofer 22 H slice on a half-specimen at 900 ^{o}C. Note that a half-specimen is a Crofer 22 H slice spread with the GC-9 glass-ceramic sealant. In order to investigate the effect of number of initial spreading side on the bonding strength of a joint, a half-specimen was placed on another half-specimen to form a specimen (HT900D and POHT900D) with a double layer of glass-ceramic sealant through the same joining heat treatment. After joining treatment, the HT900D and POHT900D specimens were tested under shear and tensile loading at both RT and 800 ^{o}C.

The shear strength of the joint specimens with a double layer of glass-ceramic sealant is shown in Fig. 23. For the HT900D specimens, the average shear strength at RT was about 6.6 MPa and decreased to about 4.7 MPa at 800 ^{o}C. For the POHT900D specimens, the average shear strength at RT was about 7 MPa and also decreased to about 4.4 MPa at 800 ^{o}C. For the double-layer joint specimens, it is also noted that a 2-h pre-oxidization heat treatment of the metallic interconnect did not significantly improve the shear joint strength, as shown in Fig. 23. This is consistent with the trend in single-layer specimens (Fig. 15). The softening behavior of the glass-ceramic sealant at 800 ^{o}C was also observed in these two cases. Comparison of the shear strength between the specimens of single and double layers of glass-ceramic sealant is shown in Fig. 24. It is generally seen that the shear strength was increased for the double-layer specimens at both as-received and pre-oxidized conditions as compared to the single-layer ones.

The typical force-displacement curves for all the tensile specimens tested at RT and 800 ^{o}C are shown in Fig. 25. The force-displacement curves at both RT and 800 ^{o}C exhibited a typical brittle fracture pattern. Figure 26 shows the tensile strength of the joint specimens with a single layer of glass-ceramic sealant. For the HT900S specimens, the tensile strength at RT was about 16.7 MPa and decreased to about 4.3 MPa at 800 ^{o}C. The tensile strength of the POHT900S specimens tested at RT was 16.8 MPa and decreased to about 5.9 MPa at 800 ^{o}C. The average tensile strength of the joint specimens with a double layer of glass-ceramic sealant is shown in Fig. 27. For the HT900D specimens, the tensile strength at RT was about 23 MPa and decreased to about

12.7 MPa at 800 ^{o}C. For the POHT900D specimens, the tensile strength at RT was about 16.7 MPa and decreased to about 12.6 MPa at 800 ^{o}C. Once again, a 2-h pre-oxidization heat treatment did not significantly enhance the tensile joint strength for both the single- and double-layer specimens. In comparison of the tensile joint strength between the single- and double-layer specimens, it is seen that the tensile joint strength was increased due to a double layer, as shown in Fig. 28. In particular, a 195% and 113% increment of tensile strength was observed for the HT900D and POHT900D specimens tested at 800 ^{o}C, respectively.

Typical failure patterns for the shear specimens of HT900D tested at RT and 800 ^{o}C are shown in Fig. 29. In Fig. 29(a), there is a shining region in the middle of the lower Crofer 22 H substrate and the chromia layer was peeled from the lower substrate. It indicates that delamination between the chromia layer and the Crofer 22 H substrate dominates the failure of HT900D at RT. For the HT900D specimens tested at 800 ^{o}C (Fig. 29(b)), it can be seen that in addition to delamination at interfaces, fracture even took place in the glass-ceramic substrate. The fracture modes of the shear specimens with a double-layer of GC-9 sealant are similar to those of a single layer. Representative failure patterns for the shear specimens of POHT900D tested at RT and 800 ^{o}C are shown in Fig. 30. For the specimens tested at RT, delamination between the chromia layer and the Crofer 22 H substrate was observed. For the specimens tested at 800 ^{o}C, fracture occurred at the interface between the glass-ceramic substrate and chromate. The failure patterns for the shear specimens of POHT900D are comparable with those of HT900D.

The fracture patterns of tensile joint specimens tested at RT and 800 ^{o}C are not as diverse as those of shear joint specimens. Figure 31 shows the typical failure patterns of tensile specimens of HT900S tested at RT and 800 ^{o}C. As shown in Fig. 31(a), fracture occurred mostly in the glass-ceramic layer. However, for the HT900S specimens tested at 800 ^{o}C, most of the fracture also occurred in the glass-ceramic substrate, while delamination was occasionally observed at the interface (Fig. 31(b)). Similar to the results of the tensile specimens without pre-oxidization treatment, fracture always occurred in the glass-ceramic layer for POHT900S specimens tested at RT (Fig. 32(a)) and fracture took place in both the glass-ceramic substrate and interface at 800 ^{o}C (Fig. 32(b)). For the HT900D tensile specimens with a double-layer of sealants, fracture took place in the glass-ceramic substrate at both RT and 800 ^{o}C, as shown in Fig. 33. As shown in Fig. 34, most of the fracture in the pre-oxidized POHT900D tensile specimens occurred in the glass-ceramic substrate at both RT

and 800 °C, while delamination was occasionally observed at the interface. These results indicate that the tensile joint strength accompanied by fracture of the glass-ceramic layer is higher than that with fracture of both the glass-ceramic layer and interface.

In the present work, a half-specimen was produced by dispensing the GC-9 slurry onto the surface of a metal slice. The half-specimen was then put in a furnace at 70 °C to dry the slurry. During joining process, the half-specimen was placed on another half-specimen or a metal slice to make a double-layer specimen or single-layer specimen, respectively. For the single-layer specimen, the pure metal slice to be joined has no spread glass initially. However, for the double-layer specimen, glass has been spread on the two metal slices before joining process. The wettability of the glass slurry initially spread on the metal slice at RT is better than that of the dry glass directly contacting the metal slice during joining at 900 °C. A good wetting behavior of glass on the metal surface can improve the joining performance. In this regard, the superiority of joint strength in double-layer specimens over that in single-layer ones was attributed to a better wetting effect. By observation of fracture in the single-layer shear specimens, fracture all occurred at the interface on the side without spread glass initially. This phenomenon is an evidence of a weaker bonding performance in the single-layer specimen. After joining at 900 °C, the thickness of glass-ceramic sealant in double-layer tensile joint specimens is about 0.44 mm and larger than that in single-layer ones, 0.22 mm. If the thickness of glass-ceramic sealant is too thin, fracture is easier to occur at interface at 800 °C. This effect also affects the tensile joint strength. For the tensile specimens tested at 800 °C, a considerable increase of tensile strength was observed for a double layer of glass-ceramic sealant as a result of a greater sealant thickness. For both single-layer and double-layer shear joint specimens, the thickness of glass-ceramic sealant is 0.5 mm. In this regard, shear strength of the joint specimens was only affected by the wettability of glass in contact with the metal surface.

3.4 Effect of Aging Treatment on the Joint Strength

As sealants used in SOFC are exposed to an oxidizing environment during operation, it is important to understand the aging effect on the joint strength at elevated temperature. In this study, some of the joined specimens were aged in air at operating temperature of 800 °C for 250, 500 and 1000 h (HT900D-A250, HT900D-A500, and HT900D-A1000, respectively) to assess the effect of aging

treatment on mechanical integrity of the joint. After aging treatment, the aged specimens were tested under shear loading at 800 ^{o}C.

The shear strength of the joint specimens aged in air is plotted in Fig. 35, in which the strength data of the unaged specimens were taken from Fig. 23. For the HT900D-A250 and HT900D-A500 specimens, the average shear strength at 800 ^{o}C was about 3.9 MPa. For the HT900D-A1000 specimens, the average shear strength was slightly decreased to 3.8 MPa. In general, the strength of the joint specimens aged to different degrees was comparable. Compared to the shear strength of the unaged specimens, a 17-19% reduction of strength was clearly observed for the aged ones. However, a longer aging treatment from 250 to 500 and 1000 h did not degrade the joint strength to a greater extent. In this regard, if the reduction of shear joint strength is maintained at 19% for aging time longer than 1000 h, the given GC-9 glass-ceramic sealant is expected to show an acceptable long-term stability of mechanical strength.

Figure 36 shows the typical failure patterns of the aged specimens tested at 800 ^{o}C. In Figs. 36(a) and 36(b), the fracture patterns of HT900D-A250 and HT900D-A500 are comparable. As shown in Fig. 36(a), there is a yellow region in the middle of the lower Crofer 22 H substrate, and there is a white region with a similar shape to the yellow region in the upper half on the surface of the glass-ceramic substrate. The yellow region is a chromate layer which was peeled from the surface of the glass-ceramic substrate. For the shear specimens of HT900D-A1000, fracture occurred in the glass-ceramic substrate and the color of the glass-ceramic substrate turned into brown from white (Fig. 36(c)). This is different from that of those aged with a shorter time (250 and 500 h) in Figs. 36(a) and 36(b). Although the fracture pattern was changed for a longer aging treatment (1000 h), the joint strength was not significantly changed compared to that with shorter aging times (250 and 500 h).

In the joining process at high temperature, $BaCrO_4$ chromate was formed on the surface of the glass-ceramic sealant. Due to the high CTE of chromate (22-23 $\times$ 10^{-6} $^{o}C^{-1}$), high thermal stresses are expected to generate cracks during cooling [9,20]. After an aging treatment, the amount of chromate in an aged specimen became greater, as compared to the as-received one. The strength degradation of aged specimens was attributed to the extensive growth of chromate. For the specimens of HT900D-A250 and HT900D-A500, fracture occurred at the interface between the chromate and the glass-ceramic substrate and the chromate was uniformly peeled off, as shown in Fig. 36. A greater extent of crystallization in the 1000-h aged specimens was expected to generate a higher strength in the glass-ceramic substrate. However, in the study of Liu

et al. [22], micro-voids due to CTE difference between the ceramic and glass phases were formed in the aged samples during a cooling process. For the HT900D-A1000 specimens, fracture took place in the glass-ceramic substrate resulting from growth of micro-voids. Typical SEM micrographs of fracture surface on the glass-ceramic layer in the shear specimens of HT900D, HT900D-A500, and HT900D-A1000 tested at 800 ^{o}C are shown in Figs. 37. As shown in Fig. 37(a), on the fractured glass-ceramic layer in the specimen of HT900D, needle-shape crystals and aggregated particles were observed and interfacial delamination was along these needle-shape crystals. As shown in Figs. 37(b) for the case of HT900D-A500, needle-shape crystals and aggregated particles were also observed and the amount of aggregated particles is greater than that of HT900D in Fig. 37(a). As shown in Fig. 37(c), the amount of aggregated particles in HT900D-A1000 was much greater than those in HT900D and HT900D-A500. As the fracture in HT900D-A1000 specimens took place within the glass-ceramic layer instead at the interface, needle-shape crystals were not found on the fracture face (Fig. 37(c)). In addition, a considerable amount of micro-voids were found between the aggregated particles and glass phase in HT900D-A1000. These micro-voids presumably caused the fracture to take place in the glass-ceramic substrate.

The SEM micrographs of a cross section of the interface between the GC-9 and Crofer 22 H in HT900D-A250, HT900D-A500, and HT900D-A1000 joint specimens are shown in Fig. 38. At the interface, there appeared two distinct zones; the upper zone in the figure represents the glass-ceramic sealant, while the lower region is the Crofer 22 H. A good physical compatibility between these two materials is observed at the interface. As shown in Fig 38(a), the chromia oxide (Cr_2O_3) layer on the metal side of HT900D-A250 and the chromate ($BaCrO_4$) layer is too thin to be found. For the HT900D-A500 joint specimen, a non-uniform chromia oxide layer on the metal side is clearly seen at the interface but the chromate layer can not be found, as shown in Fig. 38(b). As compared to Fig. 38(b), the chromia oxide layer in HT900D-A1000 (Fig. 38(c)) is more uniform and has a thickness about 0.4 μm. Above the chromia oxide layer in HT900D-A1000, a rough and bright layer is found. EDS analysis of this layer indicates that it contains an appreciable amount of Ba, Cr, and O and suggests that the rough layer is the $BaCrO_4$ layer. Figure 39 shows the distributions of elements in the interface of HT900D-A1000 by EDS. The scanned region is shown in Fig. 39(a). The distribution of Fe (Fig. 39(b)) is mainly located at the Crofer 22 H substrate. In Fig. 39(c), extensive diffusion of Cr into the glass-ceramic layer is observed after a long-term aging treatment.

At the regions supposed to be the oxide layers, the intensities of Cr, O and Ba (Fig. 39(c), 39(d), and 39(e)) are relatively high, as expected. In this regard, the formation of oxide layers could be confirmed. In Fig. 39(f), Si is present in both the glass ceramic and Crofer 22 H and has a high intensity of content, as expected.

3.5 Effect of Composition of Metallic Interconnect on the Joint Strength

Tables 1 and 2 list the chemical composition of two commercial ferritic stainless steels, Crofer 22 APU and Crofer 22 H, for use as interconnects in planar SOFCs. As shown in Tables 1 and 2, the main difference in chemical composition between these two metallic interconnects is the addition of Nb and W in Crofer 22 H. To compare the bonding strength of the GC-9 glass-ceramic sealant joined with these two Crofer 22 interconnect steels, Crofer 22 APU plates were used to make sandwich-like (Crofer 22 APU/GC-9/Crofer 22 APU) specimens (designated as HT900D-APU and POHT900D-APU). After joining at 900 ^{o}C, the specimens were tested under shear and tensile loading at 800 ^{o}C.

The shear strength data of joint specimens made of Crofer 22 APU are plotted in Fig. 40(a), in which the strength data of the specimens made of Crofer 22 H were taken from Fig. 23 for comparison. For the APU specimens, the average shear strength was about 3.7 MPa at 800 ^{o}C. For the pre-oxidized POHT900D-APU specimens, the average shear strength was about 3.6 MPa at 800 ^{o}C. In comparison of the shear strength between H and APU specimens, it is seen that an addition of Nb and W elements in the Crofer 22 H steel provides a greater bonding strength with the GC-9 glass-ceramic sealant.

The tensile strength results of APU joint specimens tested at 800 ^{o}C are shown in Fig. 40(b) to compare with the Crofer 22 H data taken from Fig. 27. The average tensile strength of HT900D-APU and pre-oxidized POHT900D-APU specimens was about 13.7 and 12.3 MPa at 800 ^{o}C, respectively. As shown in Fig. 40(b), the average tensile strength of the as-received APU joint specimens was comparable or slightly greater than that of H ones. However, for the pre-oxidized joint specimens, the APU specimens had a less tensile joint strength than did the H ones, similar to the case of shear joint strength. In general, comparisons made in Fig. 40 indicate that the newly developed Crofer 22 H interconnect steel improves the joining strength with the given GC-9 glass-ceramic sealant. In the study of Palcut et al. [23], Crofer 22 H and APU were oxidized at 850 ^{o}C in oxygen and their oxidization behavior was investigated. The oxide scale of Crofer 22 H was rougher than that of

Crofer 22 APU and the thickness of oxide scale in Crofer 22 H is thinner than that in Crofer 22 APU. As morphology of the oxide scale could affect the joining performance, the superiority of joint strength of Crofer 22 H specimens over that of Crofer 22 APU ones in the current study may be attributed to a rougher oxide scale on the Crofer 22 H specimens. SEM micrographs of the oxide scale in the given Crofer 22 H and APU metallic interconnect after test are shown in Fig. 41 and a typical spinel structure was observed in both steels. The grain size and amount of spinel on the surface of Crofer 22 H is grater than those of Crofer 22 APU.

Typical failure patterns for the shear specimens of HT900D-APU and POHT900D-APU tested at 800 ^{o}C are shown in Fig. 42. As shown in Figs. 42(a) and 41(b), in addition to delamination at interfaces, fracture even took place in the glass-ceramic substrate. Such failure patterns at 800 ^{o}C in the shear joint specimens of APU are comparable with those in the H ones (Figs. 29(b) and 30(b)). Figure 43 shows the typical failure patterns in the tensile specimens of APU tested at 800 ^{o}C. Similar to the failure patterns in the tensile specimens of H (Figs. 33(b) and 34(b)), most of the fracture occurred in the glass-ceramic layer for the APU tensile specimens.

3.6 Overall Comparison

In previous sections, effects of joining temperature, pre-oxidization, number of initial spreading side, aging treatment, and chemical composition of metallic interconnect on the joint strength between the given GC-9 glass-ceramic sealant and Crofer 22 steels have been discussed. An overall comparison of the joint strength, elastic properties, and fracture modes for all the given testing conditions is made and discussed in this section. Table 3 lists the shear strength, shear modulus, and fracture site for all the tested shear specimens. In calculating the shear modulus for the joint specimen, it was assumed that the measured nominal displacement was contributed only by the deformation of glass-ceramic sealants. Two typical stress-strain curves are plotted in Fig. 44(a) and the shear modulus is the slope of the linear portion in the stress-strain curves. For a given specimen preparation condition, the shear modulus of specimens tested at RT is greater than that at 800 ^{o}C, as shown in Table 6. This is attributed to a high-temperature softening behavior in the glass ceramic when the joint specimens were tested at 800 ^{o}C. As described above, three types of fracture sites were observed in the shear joint specimens. Fracture occurring in the GC-9 substrate is designated as “A” in Table 3. Fracture occurring at the

interface between the GC-9 substrate and $BaCrO_4$ layer is designated as “B”. Fracture occurring at the interface between the metal substrate and Cr_2O_3 layer is designated as “C”. If fracture involved two sites, these two fracture sites are marked together. For the shear specimens tested at RT, the joint strength of specimens with B+C fracture sites is greater than that of those with B only. For the shear specimens tested at 800 ^oC except the aged specimens, the joint strength of specimens with A+B fracture sites is greater than that of specimens with B only. Apparently, the interface between the GC-9 glass-ceramic substrate and $BaCrO_4$ chromate layer is the weakest layer to resist a shear loading for the joint specimens. For the three aged cases, there are noticeable differences in the structure of glass-ceramic sealants. Fracture of the HT900D-A250 and HT900D-A500 specimens taking place at the interface between the GC-9 substrate and $BaCrO_4$ layer is due to growth of the $BaCrO_4$ layer, while fracture of the HT900D-A1000 specimens occurring in the GC-9 substrate is due to growth of micro-voids.

Table 7 lists the tensile strength, the Young’s modulus, and fracture site for all the tested tensile specimens. Young’s modulus is calculated from the slope of the linear portion in the stress-strain curves, as shown in Fig. 44(b). For the tensile specimens tested at RT, a higher Young’s modulus corresponds to a higher tensile strength. For the tensile specimens tested at 800 ^oC, the same trend is also found. Similar to the shear specimens, fracture sites of the tensile specimens are marked “A” and “B”. However, fracture occurring at the interface between the metal substrate and Cr_2O_3 layer is not observed for the tensile joint specimens. For the tensile specimens tested at RT, the joint strength of specimens with A+B fracture sites is less than that of those with A only. For the tensile specimens tested at 800 ^oC, the joint strength of specimens with A+B fracture sites is also less than that of those with A only. These results indicate that the tensile joint strength would be lower if the fracture involved delamination at the interface between the GC-9 glass-ceramic substrate and $BaCrO_4$ chromate layer. A similar result was also found in Ref. [12]. As describe in Ref. [12], for the joint specimens of a G-18 glass and Crofer 22 APU tested under tensile loading, an interfacial fracture mode generated a lower joining strength in comparison with the case of fracture taking place within the bulk glass sealant.

For the shear and tensile joint strength results present in the current study, it is noted that scattering of the strength data for some testing conditions is quite large. It might be caused by the variation of specimen batch. The quality of the procedure in which the GC-9 glass slurry was spread on the Crofer 22 H and

APU slices might affect the joining performance of joint specimens. Therefore, the consistency of specimen preparation should be improved in the future work.

4. CONCLUSIONS

(1) In the current study, a technique of measuring the joint strength between glass ceramic and metallic interconnect at RT and 800 ^{o}C was developed. The tensile and shear strength of the joint specimens joined at 900 ^{o}C was greater than that of those joined at 850 ^{o}C. An increase of joining temperature presumably generated a better wetting behavior of the glass-ceramic sealant to improve the joining performance.

(2) With regard to the effect of pre-oxidization of metallic interconnect, a pre-oxidization treatment at 900 ^{o}C for 2 h did not significantly improve the shear and tensile strength of the GC-9/Crofer 22 joint specimens for all the given testing conditions. In addition, a longer pre-oxidization treatment of 20 h even considerably reduced the tensile joint strength at 800 ^{o}C by 45%.

(3) The joint strength of double-layer specimens was greater than that of single-layer ones due to a better wetting behavior of the GC-9 glass-ceramic sealant in contact with the metal slice during joining. In particular, for the tensile specimens tested at 800 ^{o}C, as the thickness of a single-layer of glass-ceramic sealant is half of the double-layer one, fracture is easier to occur at interface and a considerable strength reduction (>53%) was observed.

(4) An aging treatment at 800 ^{o}C for 250 or 500 h degraded the shear joint strength at 800 ^{o}C by 17%. A longer aging time of 1000 h further reduced the shear joint strength by a smaller, additional effect from 17% to 19%. If such a 19% reduction of shear joint strength at 800 ^{o}C is acceptable, the given GC-9 glass-ceramic sealant is expected to show an acceptable long-term stability of mechanical strength for SOFC operation.

(5) The newly developed Crofer 22 H interconnect steel exhibited a better joining strength with the given GC-9 glass-ceramic sealant, as compared to the previously developed Crofer 22 APU alloy.

(6) Three types of fracture modes were observed in the shear specimens. Firstly, fracture occurred at the interface between the glass-ceramic substrate and the chromate layer, for a low level of joint strength. Secondly, fracture occurred at the interface between the GC-9 substrate and $BaCrO_4$ layer as well as in the GC-9 substrate, for a medium level of joint

strength. Thirdly, for a high level of joint strength, fracture might take place at the interface between the metal substrate and the Cr_2O_3 layer as well as at the interface between the GC-9 substrate and $BaCrO_4$ layer.

(7) For the tensile joint specimens, a greater joint strength corresponds to fracture occurring only in the glass-ceramic sealant layer. For a lower tensile joint strength, delamination at the interface between the GC-9 substrate and $BaCrO_4$ layer was also involved in the fracture in addition to the fracture of the glass-ceramic layer.

REFERENCES

1. W. Z. Zhu and S. C. Deevi, "A Review on the Status of Anode Materials for Solid Oxide Fuel Cells," *Materials Science and Engineering*, Vol. A362, 2003, pp. 228-239.
2. J. Malzbender, J. Mönch, R. W. Steinbrech, T. Koppitz, S. M. Gross, and J. Remmel, "Symmetric Shear Test of Glass-Ceramic Sealants at SOFC Operation Temperature," *Journal of Materials Science*, Vol. 42, 2007, pp. 6297-6301.
3. T. L. Wen, D. Wang, M. Chen, H. Tu, Z. Lu, Z. Zhang, H. Nie, and W. Huang, "Material Research for Planar SOFC Stack," *Solid State Ionics*, Vol. 148, 2002, pp. 513-519.
4. J. W. Fergus, "Sealants for Solid Oxide Fuel Cells," *Journal of Power Sources*, Vol. 147, 2005, pp. 46-57.
5. P. A. Lessing, "A Review of Sealing Technologies Applicable to Solid Oxide Electrolysis Cells," *Journal of Materials Science*, Vol. 42, 2007, pp. 3465-3476.
6. C.-K. Lin, T.-T. Chen, Y.-P. Chyou, and L.-K. Chiang, "Thermal Stress Analysis of a Planar SOFC Stack," *Journal of Power Sources*, Vol. 164, 2007, pp. 238-251.
7. A.-S. Chen, "Thermal Stress Analysis of a Planar SOFC Stack with Mica Sealants," M.S. Thesis, National Central University, 2007.
8. C.-K. Lin, L.-H. Huang, L.-K. Chiang, and Y.-P. Chyou, "Thermal Stress Analysis of a Planar Solid Oxide Fuel Cell Stacks: Effects of Sealing Design," *Journal of Power Sources*, Vol. 192, 2009, pp. 515-524.
9. Y.-S. Chou, J. W. Stevenson, and P. Singh, "Effect of Pre-Oxidation and

Environmental Aging on the Seal Strength of a Novel High-Temperature Solid Oxide Fuel Cell (SOFC) Sealing Glass with Metallic Interconnect," *Journal of Power Sources*, Vol. 184, 2008, pp. 238-244.

10. V. A. Haanappel, V. Shemet, I. C. Vinke, and W. J. Quadakkers, "A Novel Method to Evaluate the Suitability of Glass Sealant-Alloy Combinations under SOFC Stack Conditions," *Journal of Power Sources*, Vol. 141, 2005, pp. 102-107.
11. F. Smeacetto, M. Salvo, M. Ferraris, V. Casalegno, P. Asinari, and A. Chrysanthou, "Characterization and Performance of Glass-Ceramic Sealant to Join Metallic Interconnects to YSZ and Anode-Supported-Electrolyte in Planar SOFCs," *Journal of the European Ceramic Society*, Vol. 28, 2008, pp. 2521-2527.
12. E.V. Stephensa, J.S. Vetranob, B.J. Koeppela, Y. Choua, X. Suna, and M.A. Khaleela, "Experimental Characterization of Glass-Ceramic Seal Properties and their Constitutive Implementation in Solid Oxide Fuel Cell Stack Models," *Journal of Power Sources*, Vol. 193, 2009, pp. 625-631.
13. Y.-S. Chou, J. W. Stevenson, and P. Singh, "Effect of Aluminizing of Cr-Containing Ferritic Alloys on the Seal Strength of a Novel High-Temperature Solid Oxide Fuel Cell Sealing Glass," *Journal of Power Sources*, Vol. 185, 2008, pp. 1001-1008.
14. I. W. Donald, "Preparation, Properties and Chemistry of Glass- and Glass-Ceramic-to-Metal Seals and Coatings," *Journal of Materials Science*, Vol. 28, 1993, pp. 2841-2886.
15. F. Smeacetto, M. Salvo, M. Ferraris, J. Cho, and A.R. Boccaccini, "Glass-Ceramic Seal to Join Crofer 22 APU Alloy to YSZ Ceramic in Planar SOFCs," *Journal of the European Ceramic Society*, Vol. 28, 2008, pp. 61-68.
16. Y.-T. Chiou, private communication, 2010.
17. H.-T. Chang, C.-K. Lin, and C.-K. Liu, "High-Temperature Mechanical Properties of a Glass Sealant for Solid Oxide Fuel Cell," *Journal of Power Sources*, Vol. 189, 2009, pp. 1093-1099.
18. H.-T. Chang, C.-K. Lin, and C.-K. Liu, "Effects of Crystallization on the High-Temperature Mechanical Properties of a Glass Sealant for Solid Oxide Fuel Cell," *Journal of Power Sources*, Vol. 195, 2010, pp. 3159-3165.
19. H.-T. Chang, "High Temperature Mechanical Properties of a Glass Sealant for Solid Oxide Fuel Cell," Ph.D. Thesis, National Central University, 2010.

20. C.-K. Liu, T.-Y. Yung, S.-H. Wu, and K.-F. Lin, “Study on SiO_2-B_2O_3-Al_2O_3-BaO Glass System for SOFC Applications,” *Proceedings of the MRS_Taiwan Annual Meeting 2007*, 2007 (CD-ROM). (in Chinese)
21. J.-W. Tian, “Analysis of Thermal Stresses and Mechanical Properties for the Components of Solid Oxide Fuel Cell,” M.S. Thesis, National Central University, 2009.
22. W. Liu, X. Sun, and M. A. Khaleel, “Predicting Young’s Modulus of Glass/Ceramic Sealant for Solid Oxide Fuel Cell Considering the Combined Effects of Aging, Micro-Voids and Self-Healing,” *Journal of Power Sources*, Vol. 185, 2008, pp. 1193-1200.
23. M. Palcut, L. Mikkelsen, K. Neufeld, M. Chen, R. Knibbe, and P. V. Hendriksen, “Corrosion Stability of Ferritic Stainless Steels for Solid Oxide Electrolyer Cell Interconnects,” *Corrosion Science*, 2010, doi: 10.1016/j.corsci.2010.06.006.

Table 1 Chemical composition of Crofer 22 H alloy (in wt.%)

Fe	C	Cr	Mn	Si	Ti	Nb
Bal.	0.007	22.93	0.43	0.21	0.07	0.51
Cu	S	P	Al	W	La	
0.02	<0.002	0.014	0.02	1.94	0.08	

Table 2 Chemical composition of Crofer 22 APU alloy (in wt.%)

Fe	C	Cr	Mn	Si	Ti	Cu
Bal.	0.003	22.71	0.44	0.02	0.07	0.01
S	P	Al	La			
<0.002	0.004	0.01	0.09			

Table 3 Mechanical property of Crofer 22 H alloy [16]

Temperature (^{o}C)	Yield Strength (MPa)	Ultimate Tensile Strength (MPa)	Young's Modulus (GPa)	Elongation (in 12 mm) (%)
25	406	567	205	27
600	286	359	181	29
650	241	295	161	30
700	204	219	142	39
750	140	147	88	54
800	120	123	86	55

Table 4 Mechanical property of Crofer 22 APU alloy [16]

Temperature (^{o}C)	Yield Strength (MPa)	Ultimate Tensile Strength (MPa)	Young's Modulus (GPa)	Elongation (in 12 mm) (%)
25	291	417	214	29
600	201	279	162	39
650	162	203	157	46
700	92	102	91	58
750	57	64	66	80
800	44	48	44	99

Table 5 Mean value of flexural strength and average value of Young's modulus of the non-aged, sintered GC-9 glass at various temperatures [19]

	Temperature				
	25°C	650°C	700°C	750 °C	800 °C
Flexural strength (MPa)	37	50	51	33	17
Young's modulus (GPa)	26 (8.2)	27 (4.6)	13 (3.1)	7 (2.7)	3 (1.0)

Note: value in the parentheses is the standard deviation.

Table 6 Shear strength, shear modulus, and fracture site of tested shear joint specimens

Test temperature (°C)	Specimen condition	Average shear strength (MPa)	Average shear modulus (MPa)	Fracture site*
25	HT850S	3.6	34.8	B+C
25	POHT850S	1.6	23.7	B
25	HT900S	4.9	40.2	B+C
25	POHT900S	5.6	30.7	B+C
25	HT900D	6.6	25.0	B+C
25	POHT900D	7.0	21.5	B+C
800	HT850S	4.3	14.3	B
800	POHT850S	2.4	15.7	B
800	HT900S	4.4	19.4	A+B
800	POHT900S	4.2	21.0	A+B
800	HT900D	4.7	10.3	A+B
800	POHT900D	4.4	10.4	A+B
800	HT900D-A250	3.9	13.2	B
800	HT900D-A500	3.9	12.8	B
800	HT900D-A1000	3.8	10.9	A
800	HT900D-APU	3.8	10.7	A+B
800	POHT900D-APU	3.7	10.1	A+B

*A: in glass-ceramic sealant layer; B: at the interface between the glass-ceramic substrate and $BaCrO_4$ layer; C: at the interface between the metal substrate and Cr_2O_3 layer.

Table 7 Tensile strength, Young’s modulus, and fracture site of tested tensile joint specimens

Test temperature (^{o}C)	Specimen condition	Average tensile strength (MPa)	Average Young’s modulus (MPa)	Fracture site
25	HT900S	16.7	23.2	A
25	POHT900S	16.8	45.3	A
25	HT900D	23.0	75.1	A
25	POHT900D	16.7	46.4	A+B
800	HT900S	4.3	21.7	A+B
800	POHT900S	5.9	23.2	A+B
800	HT900D	12.7	77.3	A
800	POHT900D	12.6	75.1	A+ B
800	LPOHT900D	7.0	43.1	A+ B
800	HT900D-APU	13.7	77.5	A
800	POHT900D-APU	12.3	67.2	A+ B

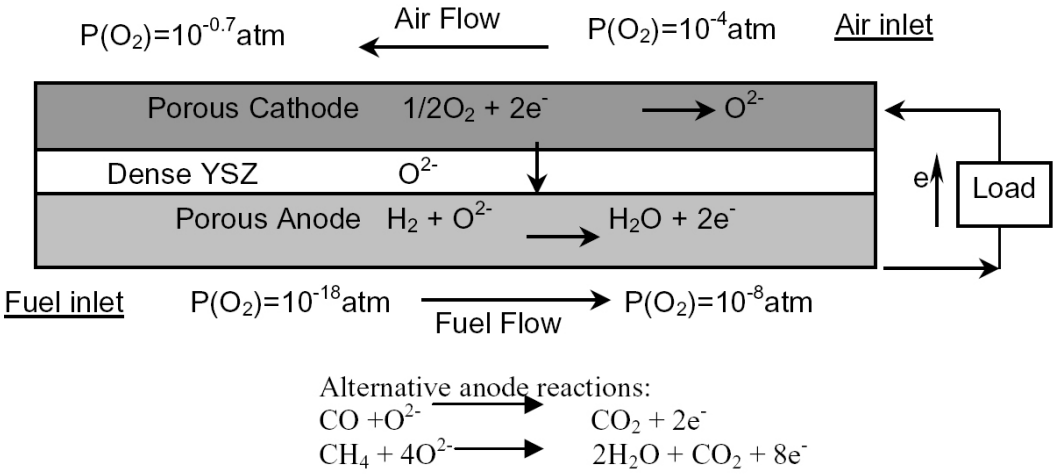

Fig. 1 Schematic of working principle for SOFC operating with hydrogen. [1]

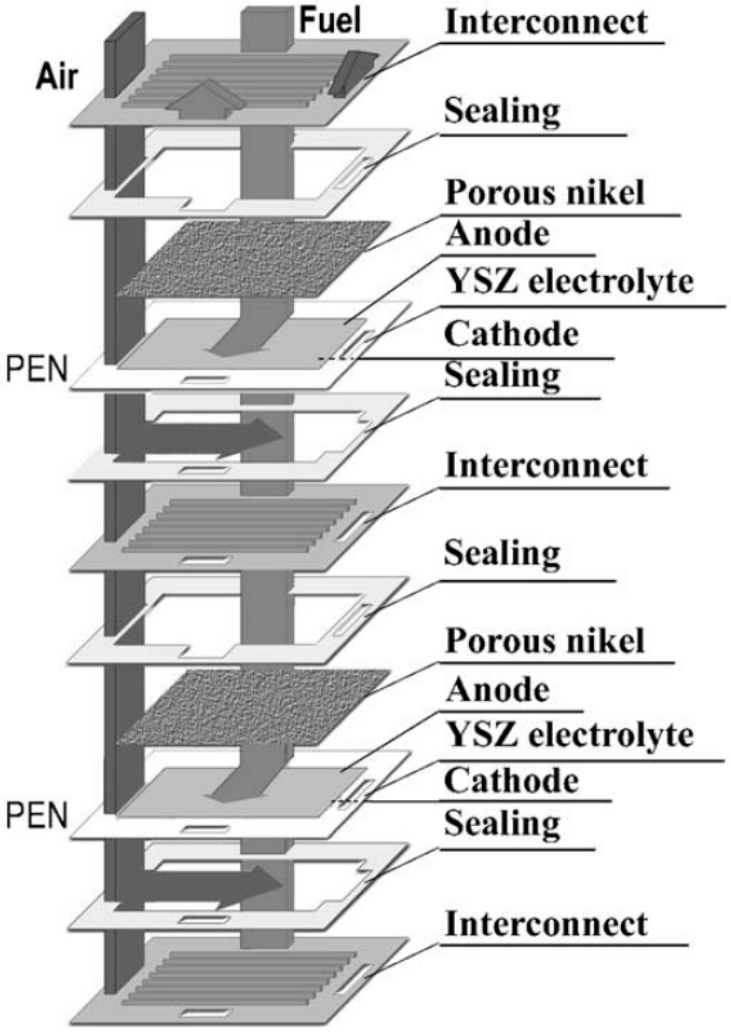

Fig. 2 Structural scheme of a planar SOFC stack. [3]

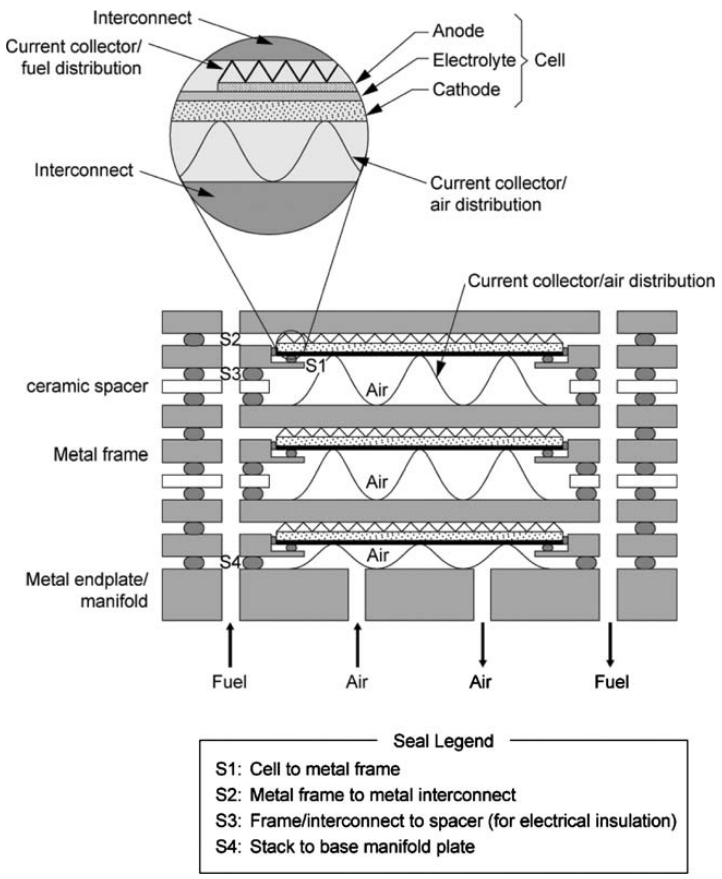

Fig. 3 Scheme of seals used in a planar SOFC stack with metallic interconnects and metallic internal gas manifold channels. [5]

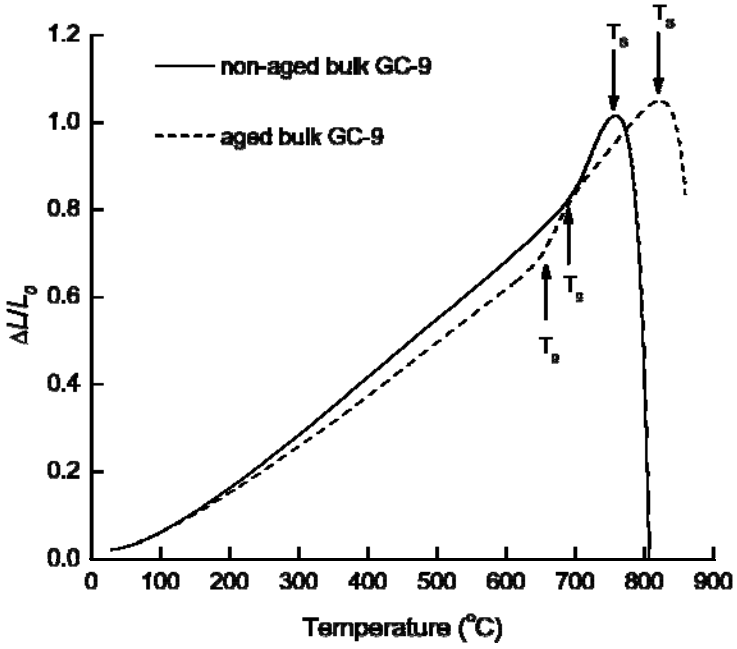

Fig. 4 Thermal expansion curves of non-aged and aged GC-9 bulk glass. [18]

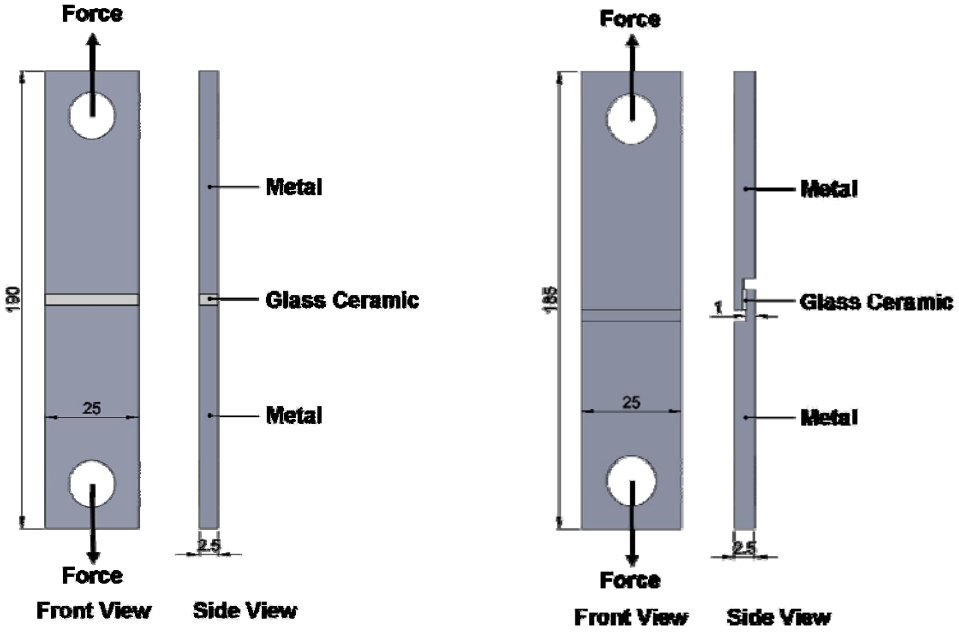

(a) (b)

Fig. 5 Scheme of two types of joint specimens: (a) tensile specimen and (b) shear specimen. (Dimensions: mm)

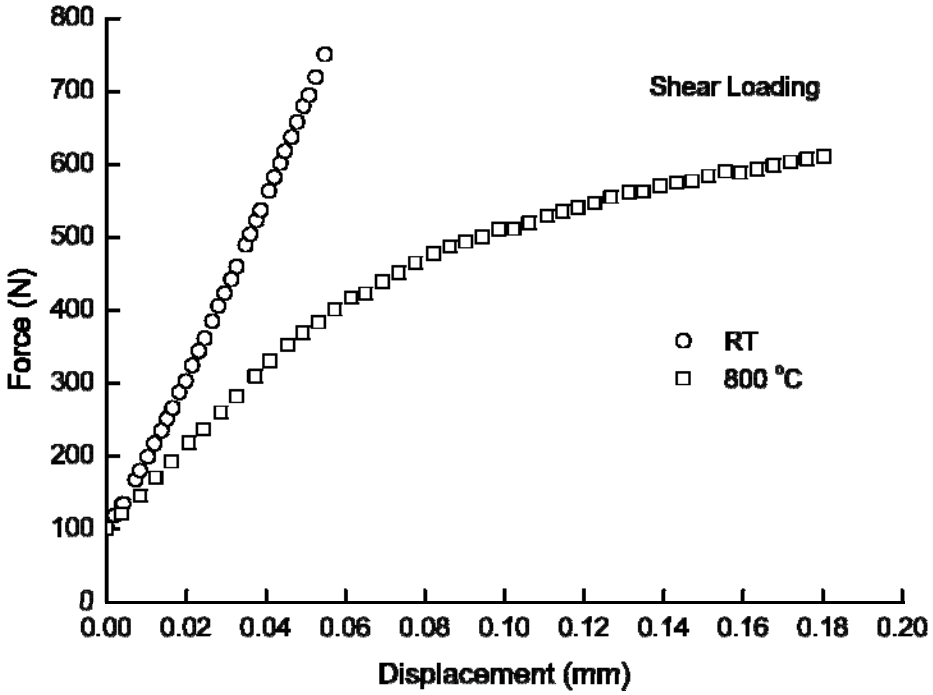

Fig. 6 Typical force-displacement curves of the joint specimens tested under shear loading at RT and 800 ^{o}C.

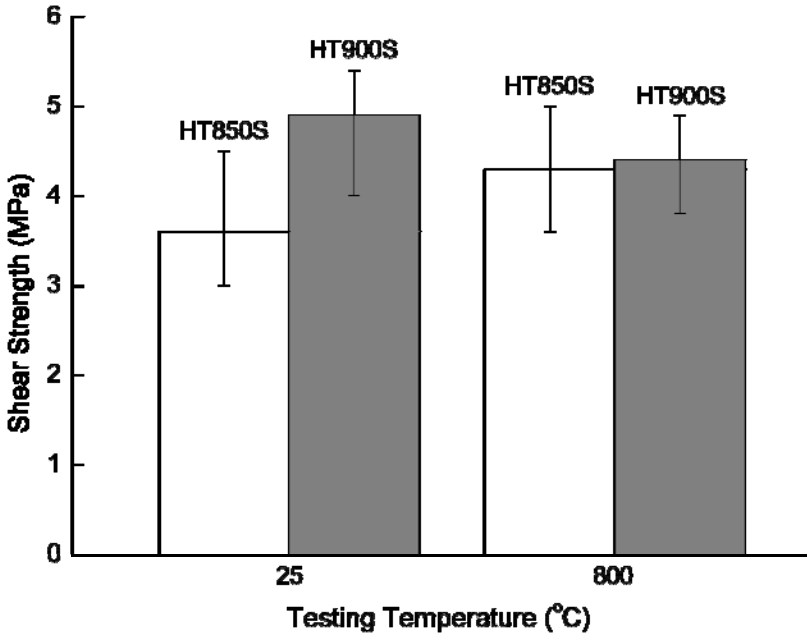

Fig. 7 Shear strength of as-received joint specimens with two different joining temperatures.

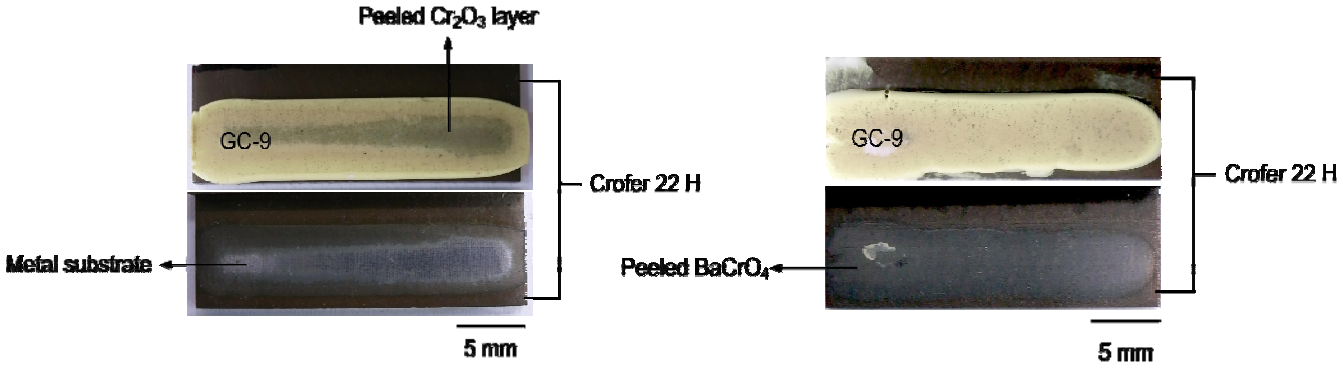

(a) (b)

Fig. 8 Failure patterns of shear specimens of HT850S tested at (a) RT [21] and (b) 800 °C.

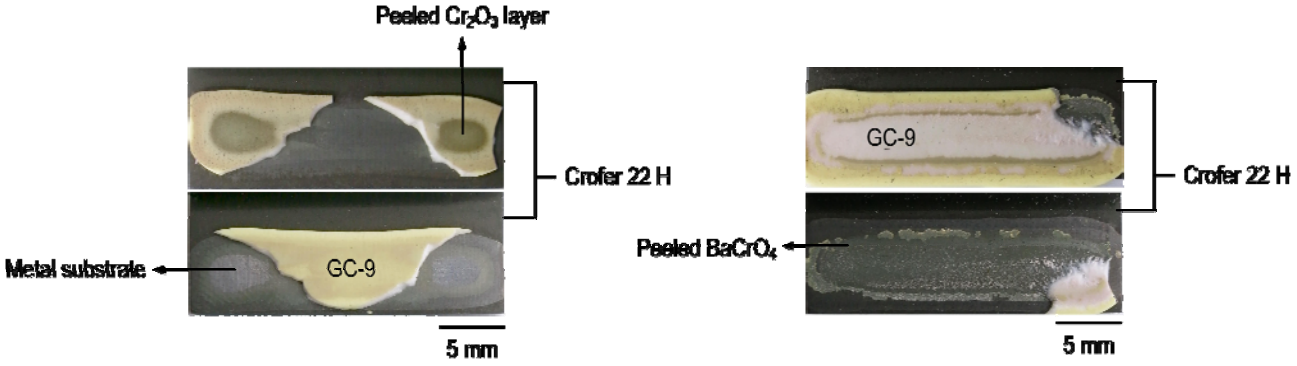

(a) (b)

Fig. 9 Failure patterns of shear specimens of HT900S tested at (a) RT and (b) 800 ^{o}C.

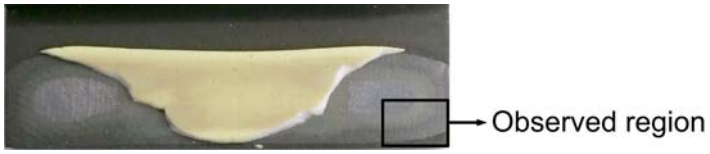

(a)

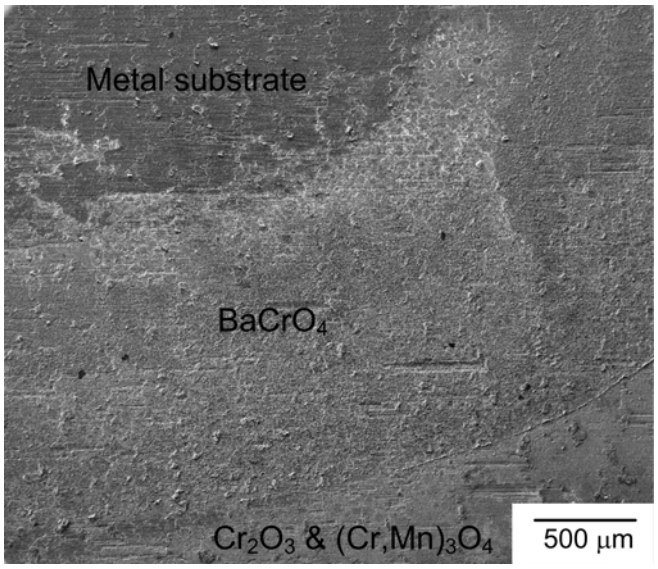

(b)

Fig. 10 A fracture surface region without adhered glass-ceramic: (a) optical micrograph showing the observed region of SEM; (b) SEM micrograph of the outlined region.

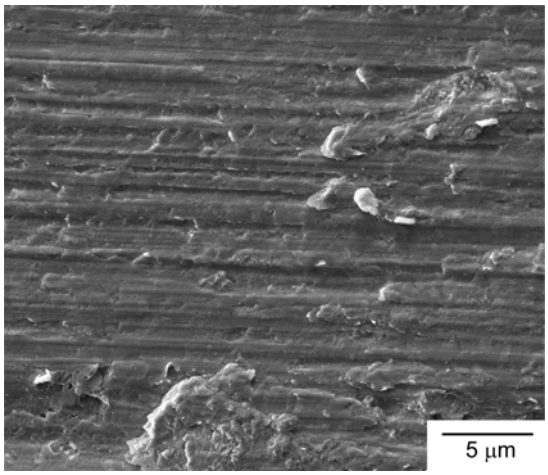

(a)

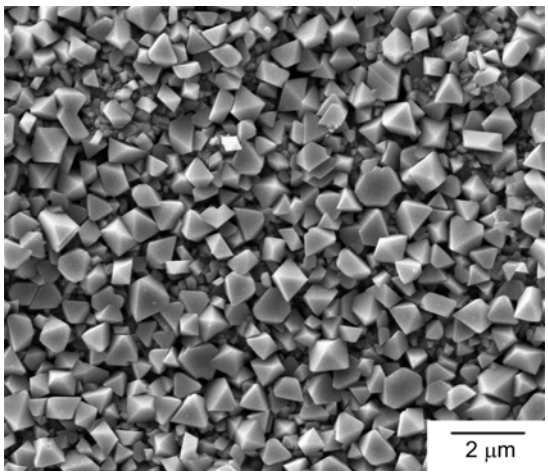

(b)

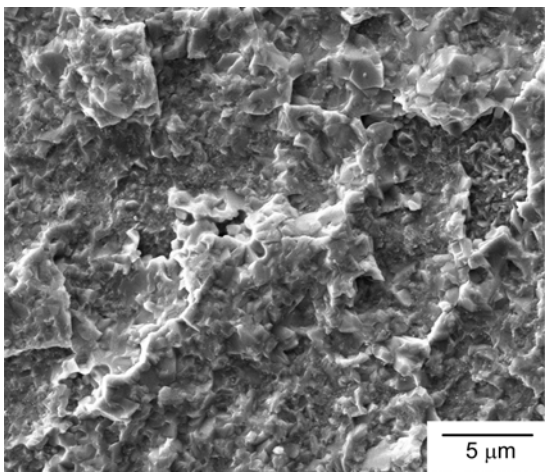

(c)

Fig. 11 SEM micrographs of a high magnification view of the three regions shown in Fig. 9: (a) metal substrate; (b) chromate ($BaCrO_4$); (c) spinel ($(Cr,Mn)_3O_4$).

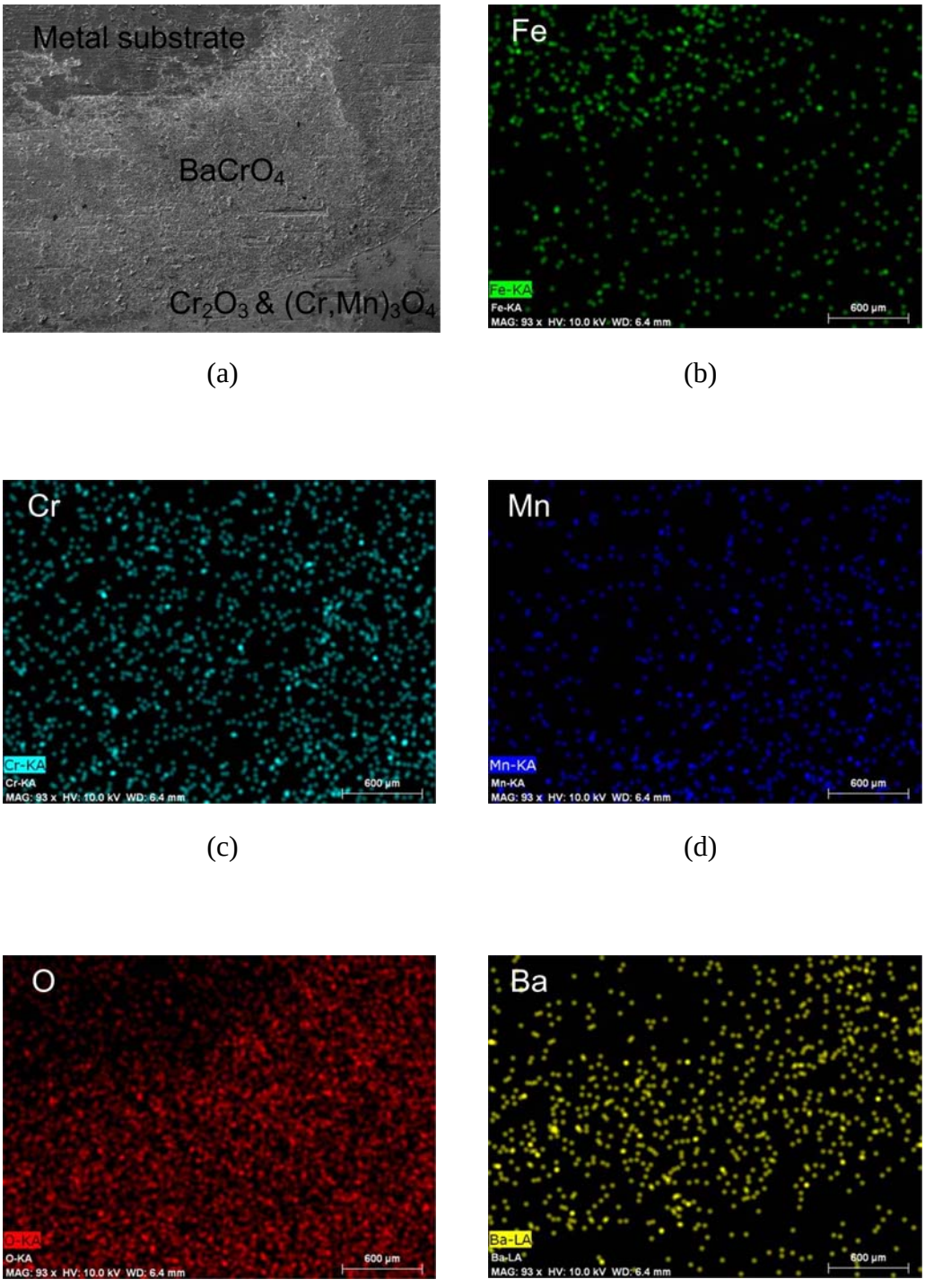

Fig. 12 EDS mapping of elements on the fracture surface region outlined in Fig. 9(b): (a) mapping region; (b) Fe; (c) Cr; (d) Mn; (e) O; (f) Ba.

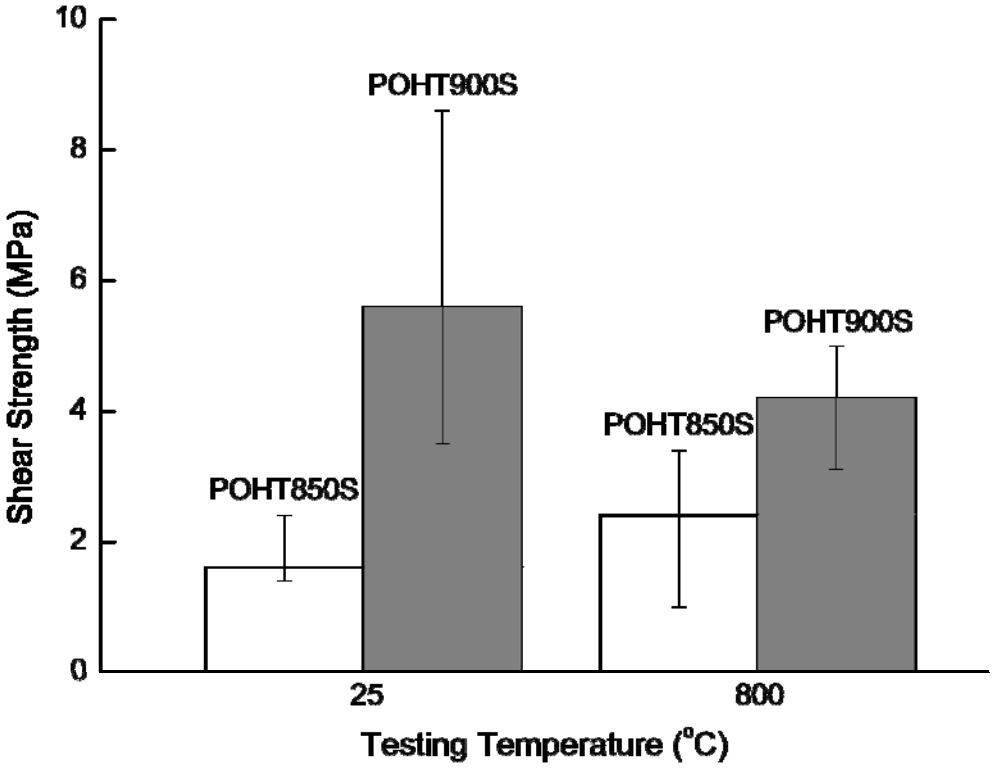

Fig. 13 Shear strength of pre-oxidized joint specimens with two different joining temperatures.

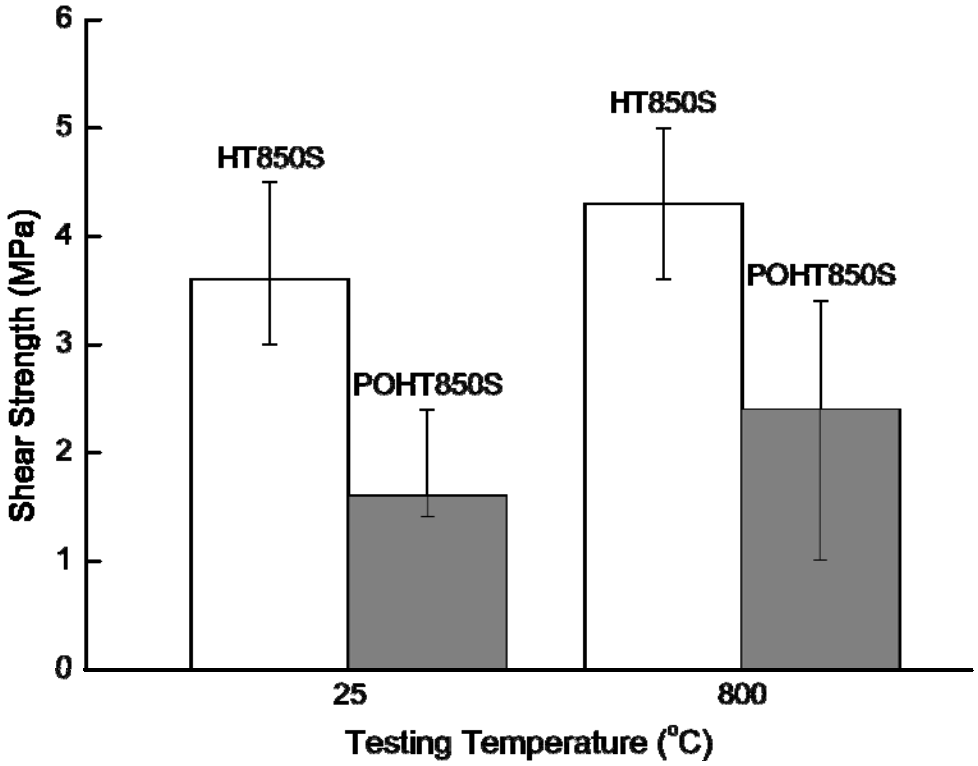

Fig. 14 Shear strength of as-received and pre-oxidized joint specimens joined at 850 °C.

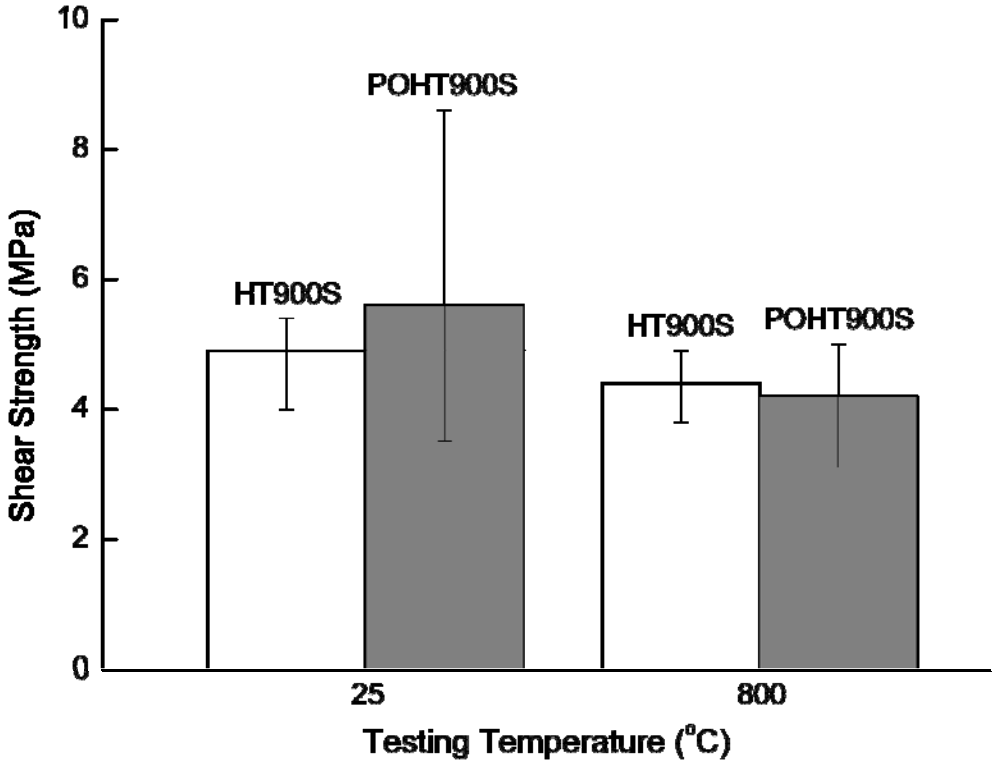

Fig. 15 Shear strength of as-received and pre-oxidized joint specimens joined at 900 °C.

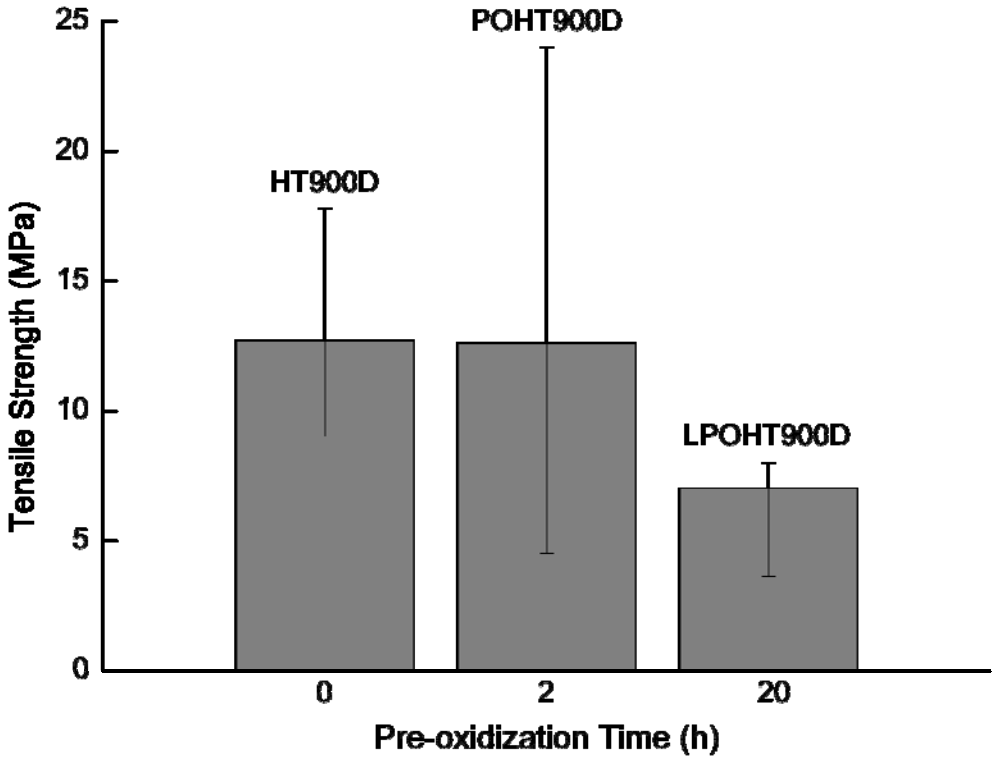

Fig. 16 Tensile strength at 800 °C for specimens joined at 900 °C with various pre-oxidization treatment times.

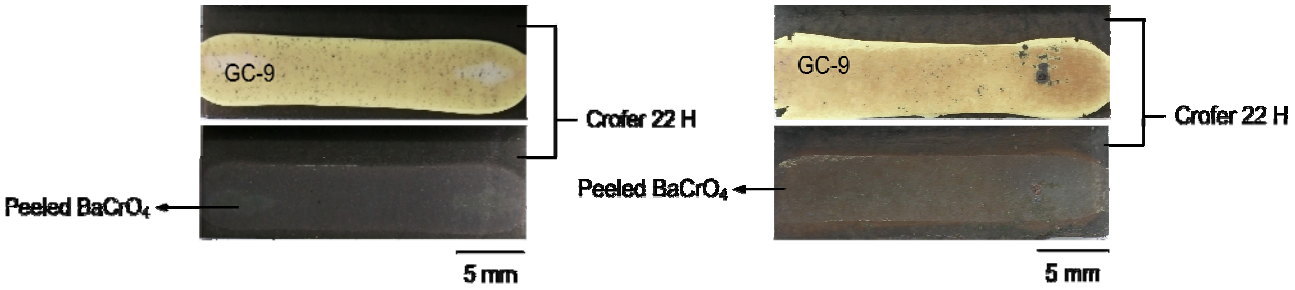

(a) (b)

Fig. 17 Failure patterns of shear specimens of POHT850S tested at (a) RT and (b) 800 ^{o}C.

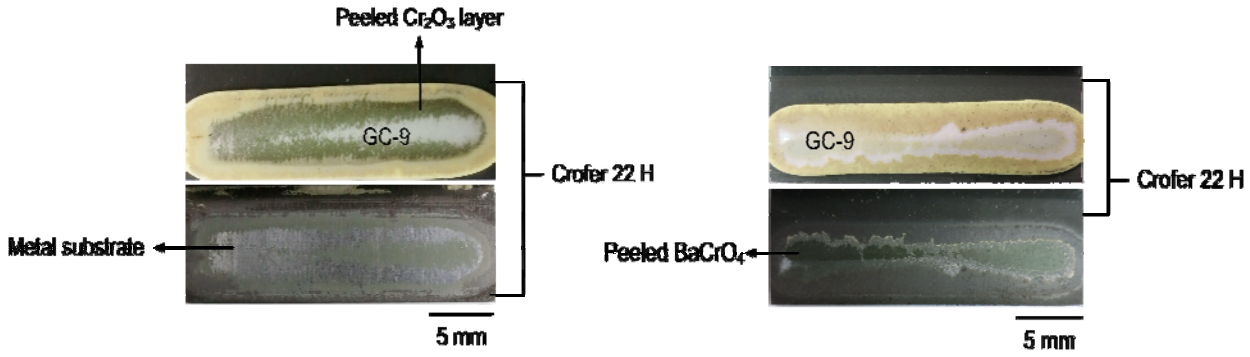

(a) (b)

Fig. 18 Failure patterns of shear specimens of POHT900S tested at (a) RT and (b) 800 ^{o}C.

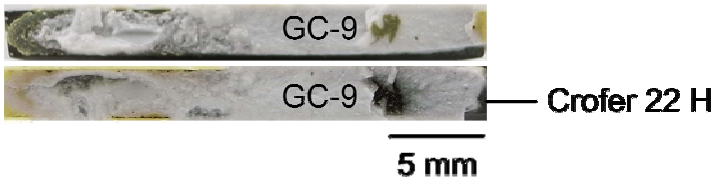

(a)

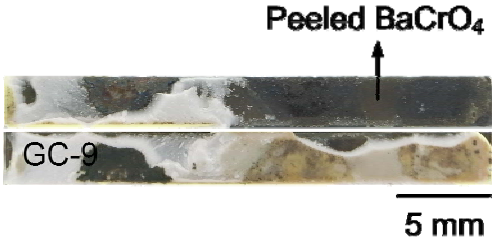

(b)

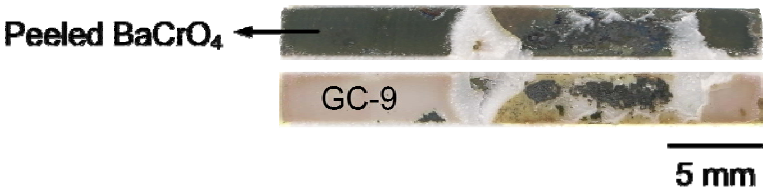

(c)

Fig. 19 Failure patterns of tensile specimens tested at 800 ^{o}C: (a) HT900D; (b) POHT900D; (c) LPOHT900D.

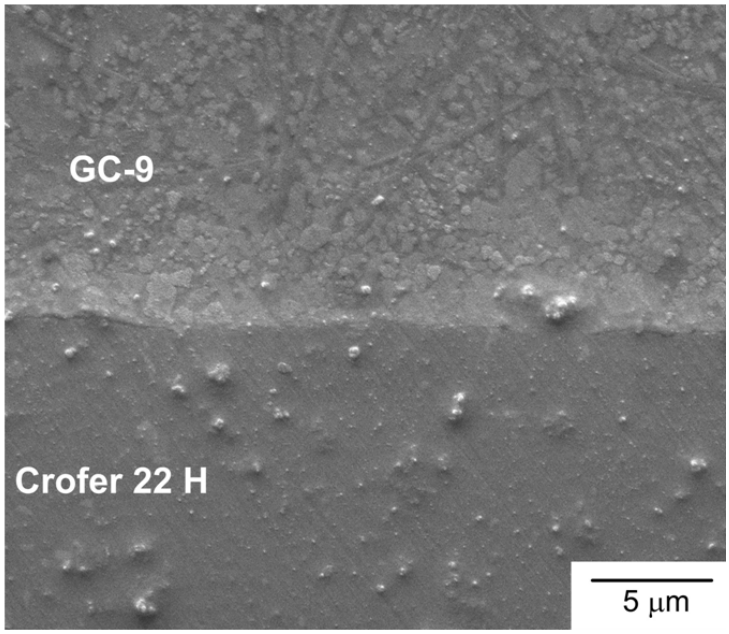

Fig. 20 SEM micrograph of a cross section of the interface between the GC-9 and Crofer 22 H in an HT900D joint specimen.

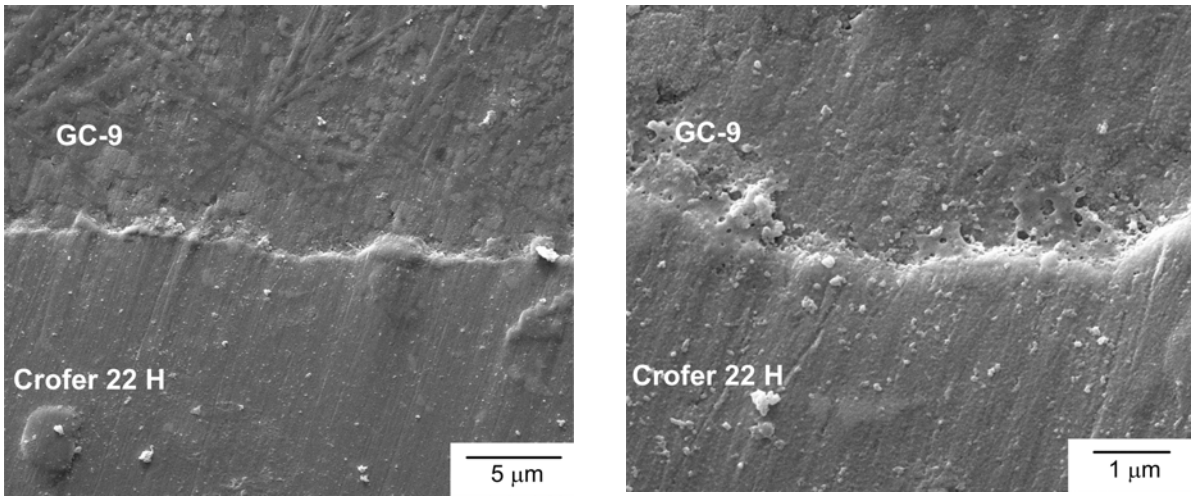

(a) (b)

Fig. 21 SEM micrographs of a cross section of the interface between the GC-9 and Crofer 22 H in a POHT900D joint specimen: (a) low magnification view; (b) high magnification view.

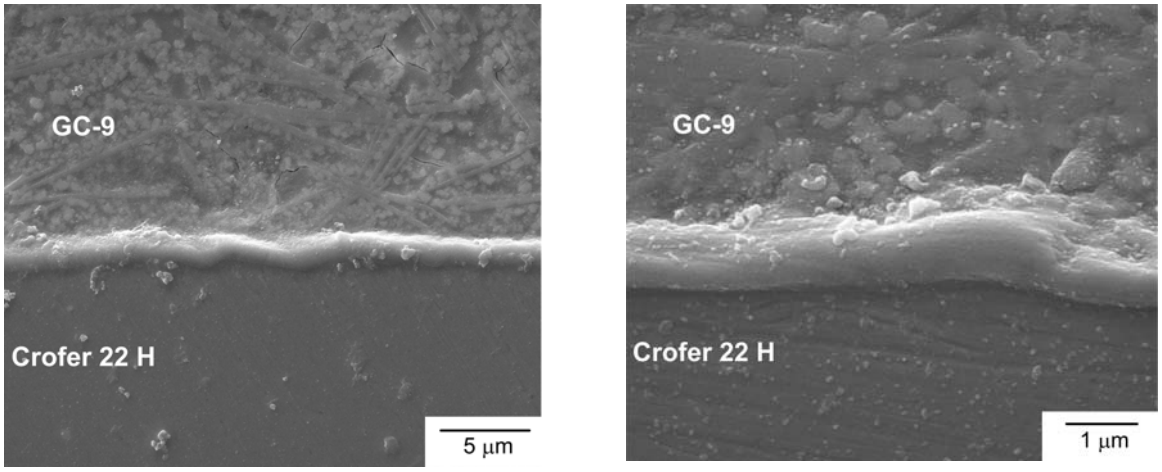

(a) (b)

Fig. 22 SEM micrographs of a cross section of the interface between the GC-9 and Crofer 22 H in an LPOHT900D joint specimen: (a) low magnification view; (b) high magnification view.

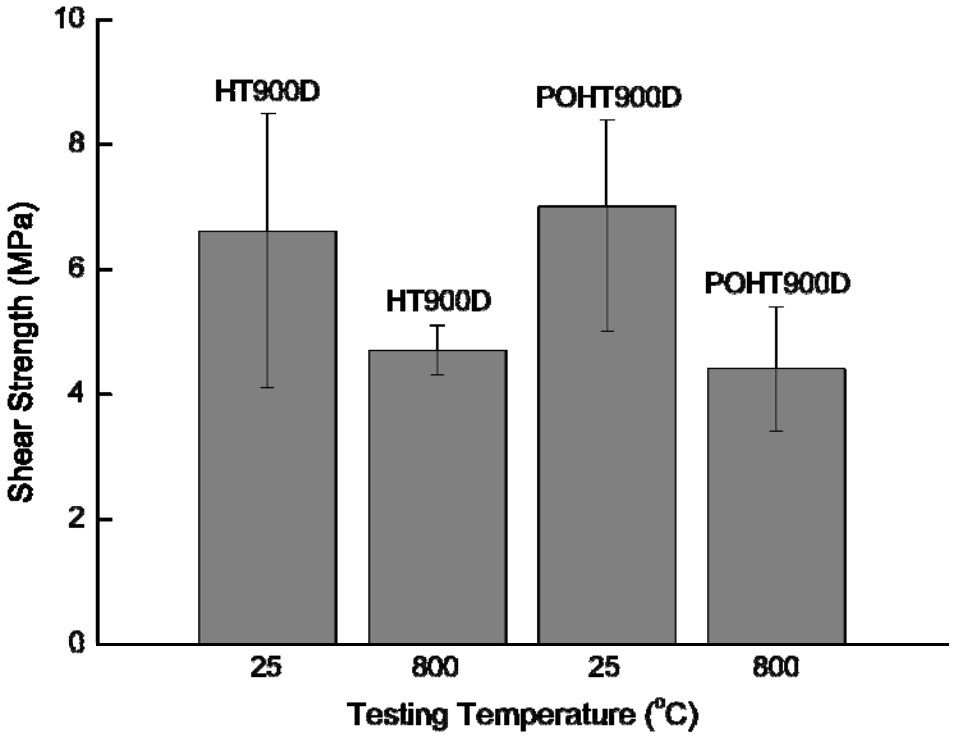

Fig. 23 Shear strength of joint specimens with a double layer of glass-ceramic sealant.

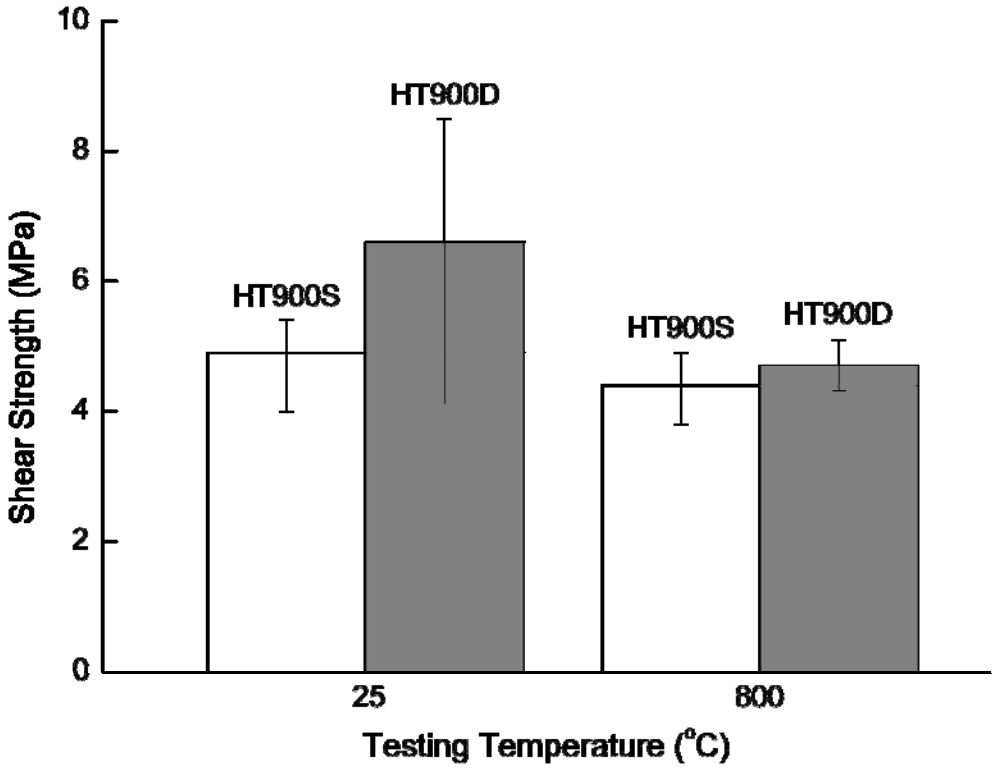

(a)

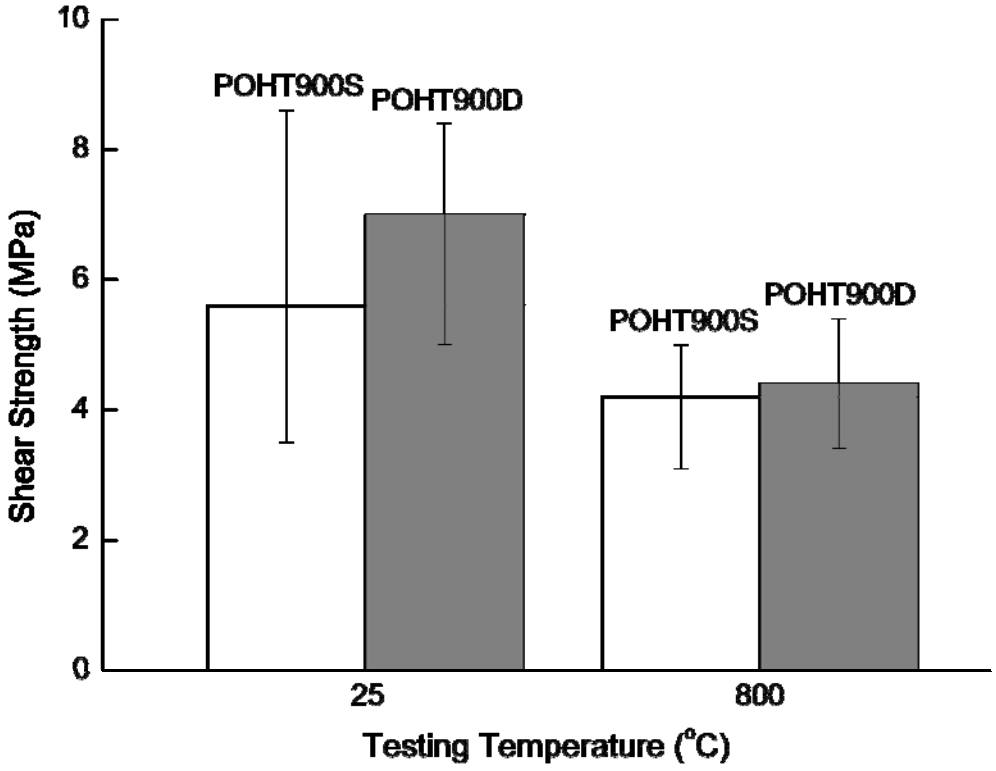

(b)

Fig. 24 Comparison of the shear strength between joint specimens with single and double layers of glass-ceramic sealant: (a) as-received; (b) pre-oxidized.

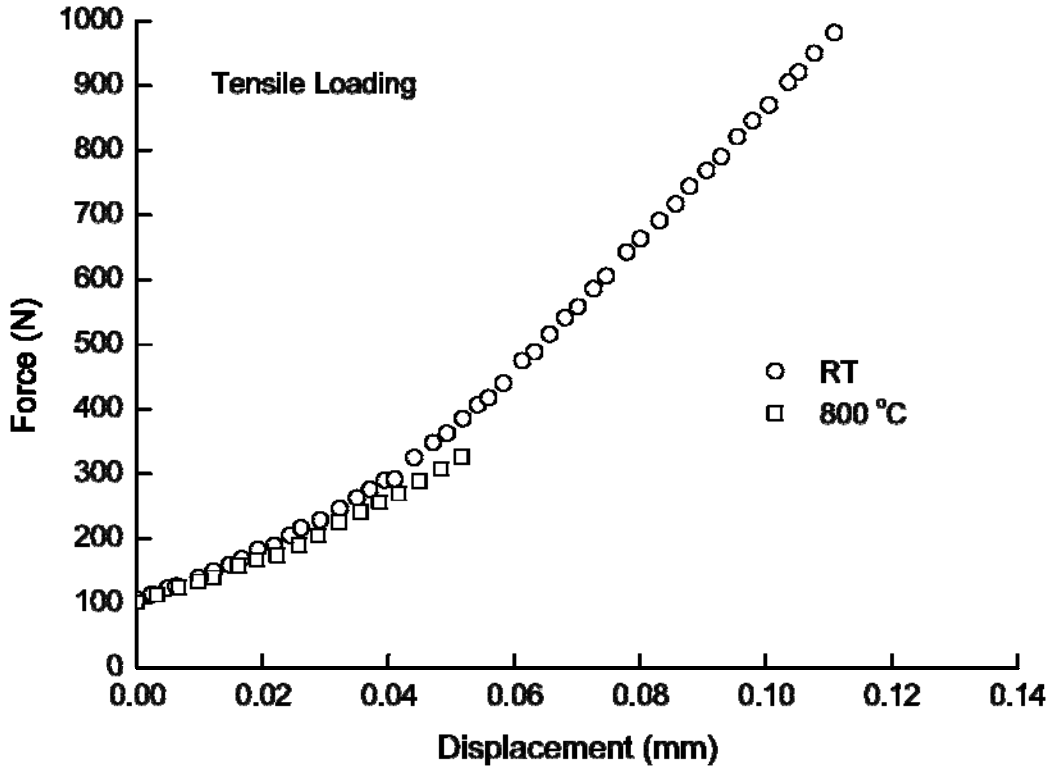

Fig. 25 Typical force-displacement curves of the joint specimens tested under tensile loading at RT and 800 ^{o}C.

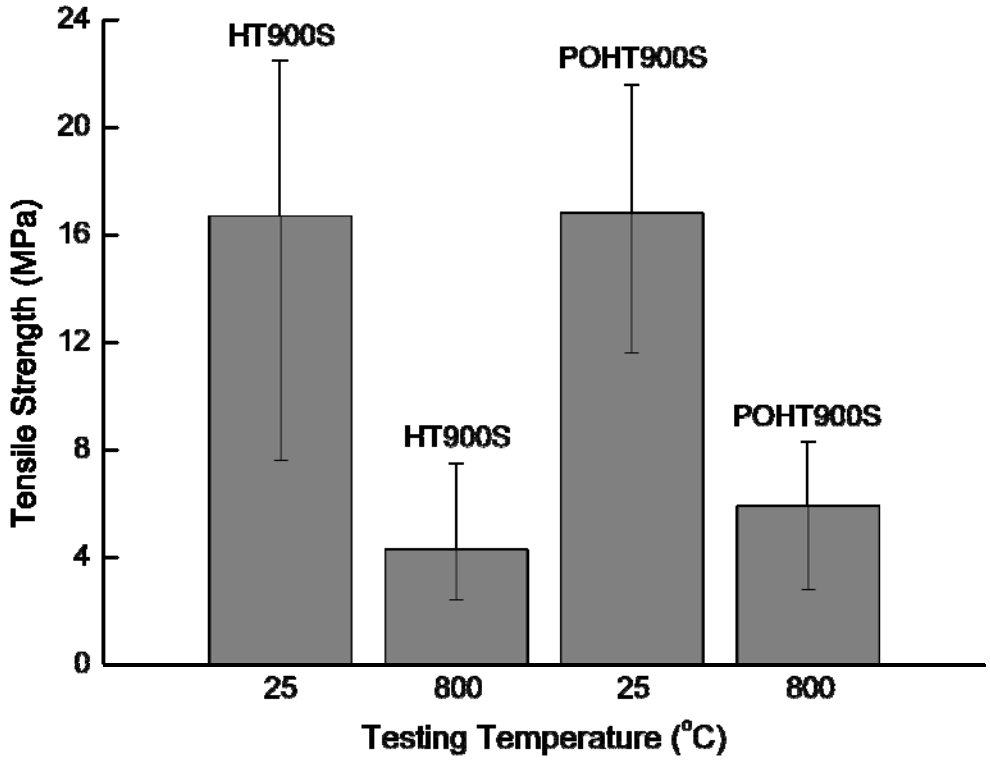

Fig. 26 Tensile strength of joint specimens with a single layer of glass-ceramic sealant.

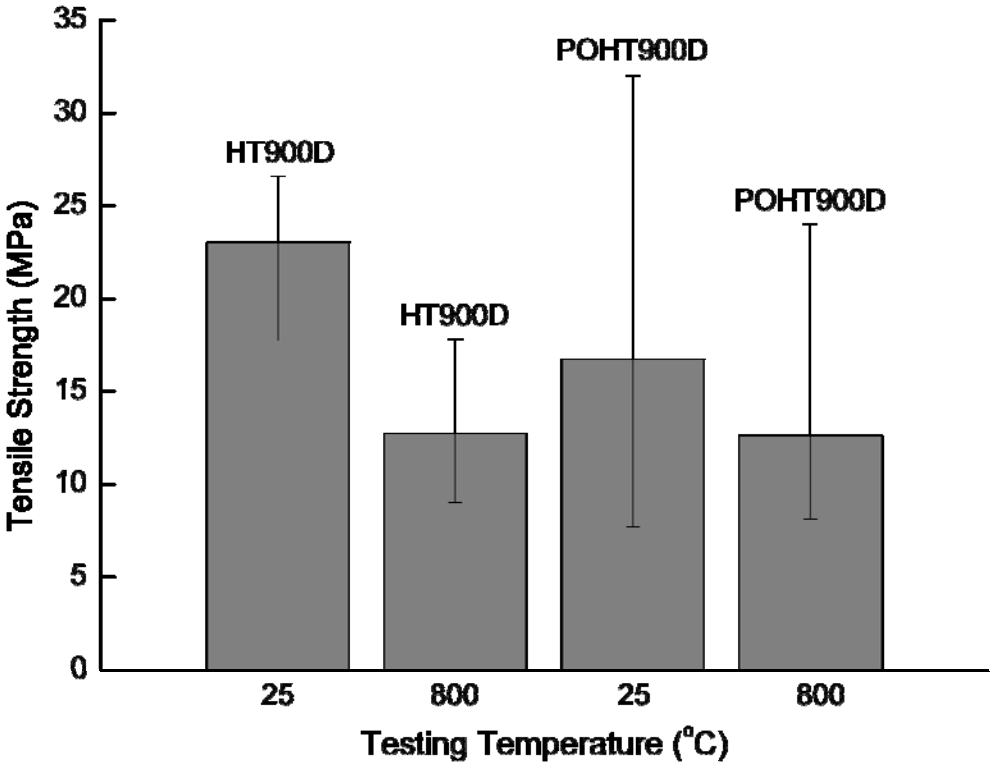

Fig. 27 Tensile strength of joint specimens with a double layer of glass-ceramic sealant.

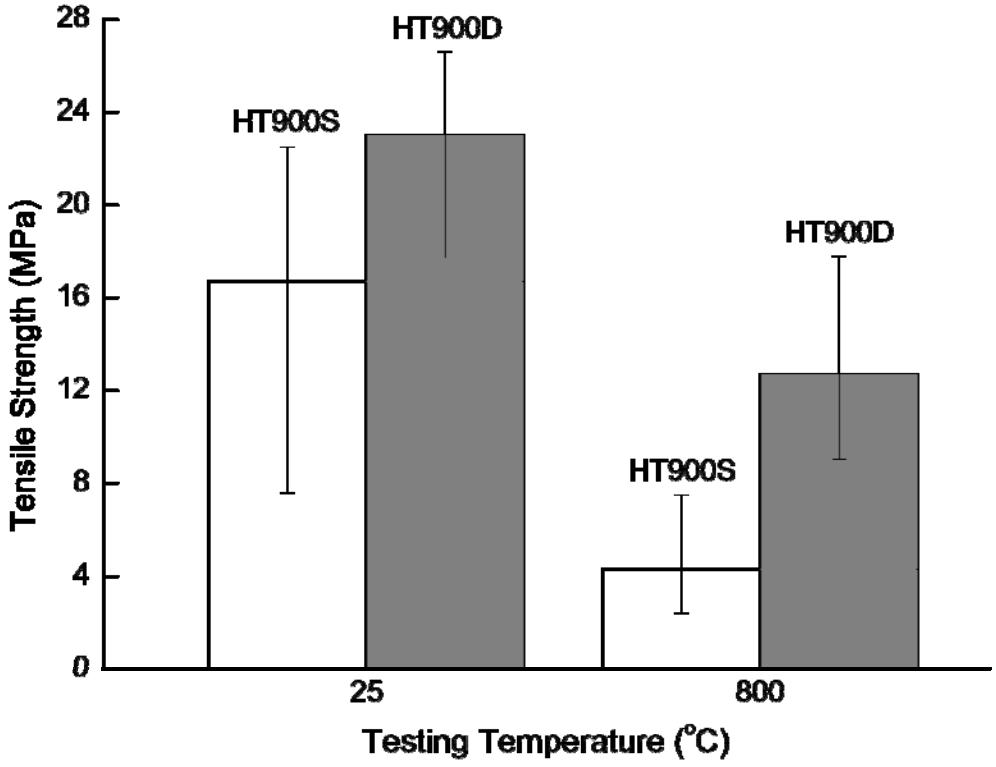

(a)

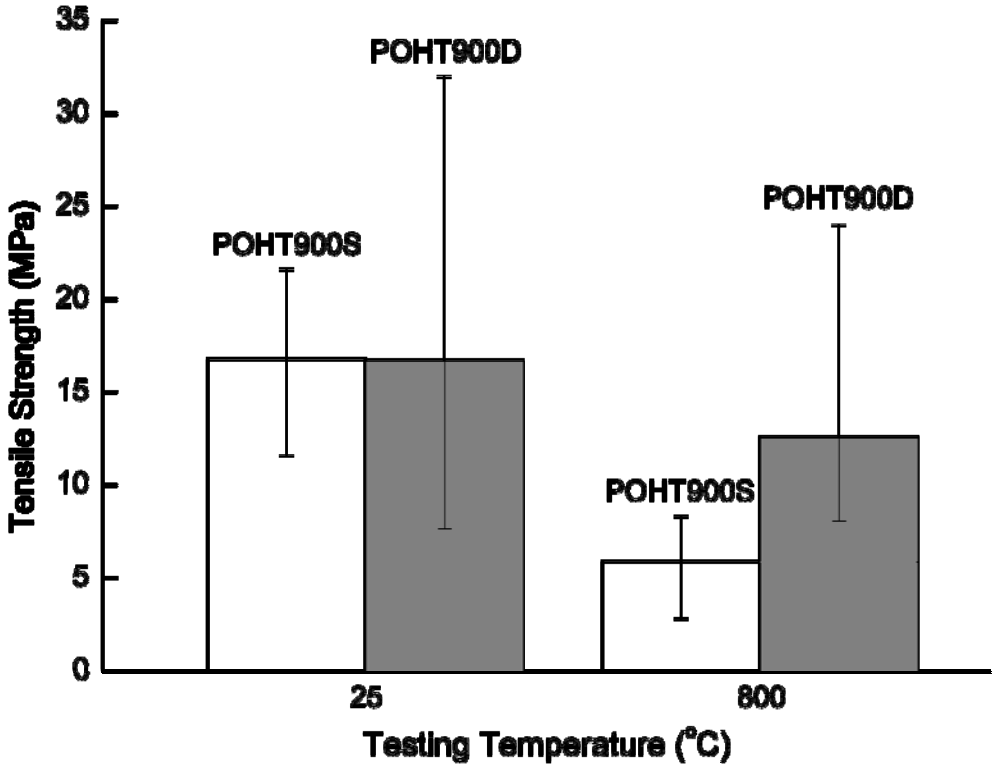

(b)

Fig. 28 Comparison of the tensile strength between joint specimens with single and double layers of glass-ceramic sealant: (a) as-received; (b) pre-oxidized.

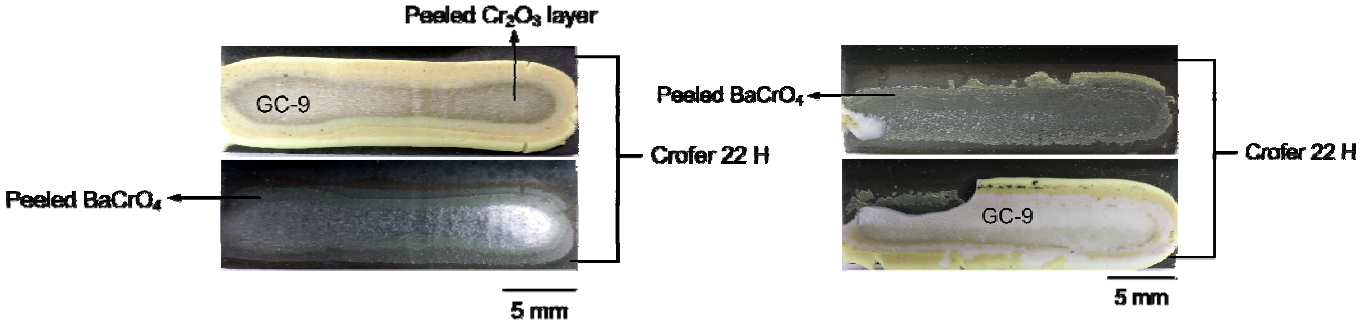

(a) (b)

Fig. 29 Failure patterns of shear specimens of HT900D tested at (a) RT and (b) 800 ^{o}C.

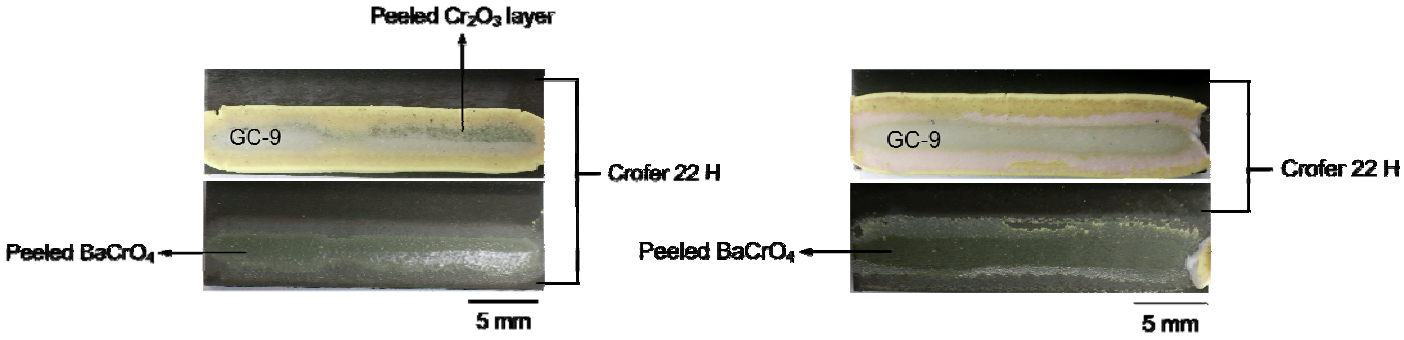

(a) (b)

Fig. 30 Failure patterns of shear specimens of POHT900D tested at (a) RT and (b) 800 ^{o}C.

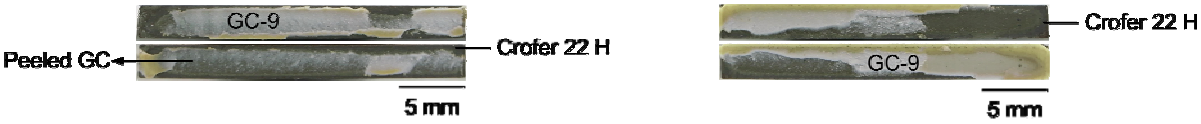

(a) (b)

Fig. 31 Failure patterns of tensile specimens of HT900S tested at (a) RT and (b) 800 ^{o}C.

(a) (b)

Fig. 32 Failure patterns of tensile specimens of POHT900S tested at (a) RT and (b) 800 ^{o}C.

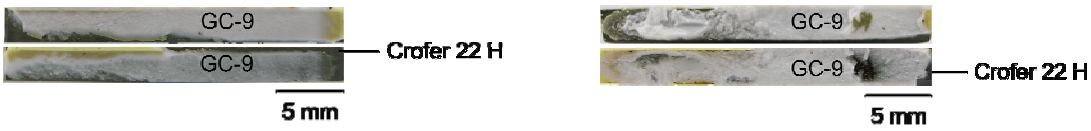

(a) (b)

Fig. 33 Failure patterns of tensile specimens of HT900D tested at (a) RT and (b) 800 ^{o}C.

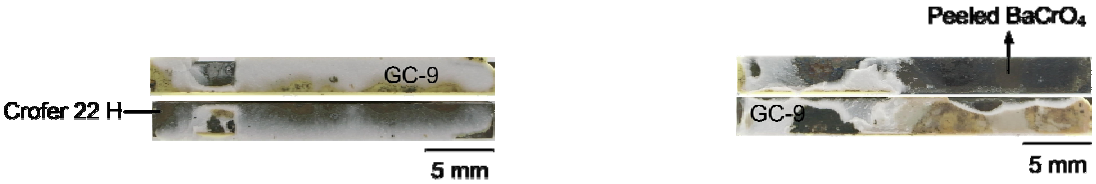

(a) (b)

Fig. 34 Failure patterns of tensile specimens of POHT900D tested at (a) RT and (b) 800 ^{o}C.

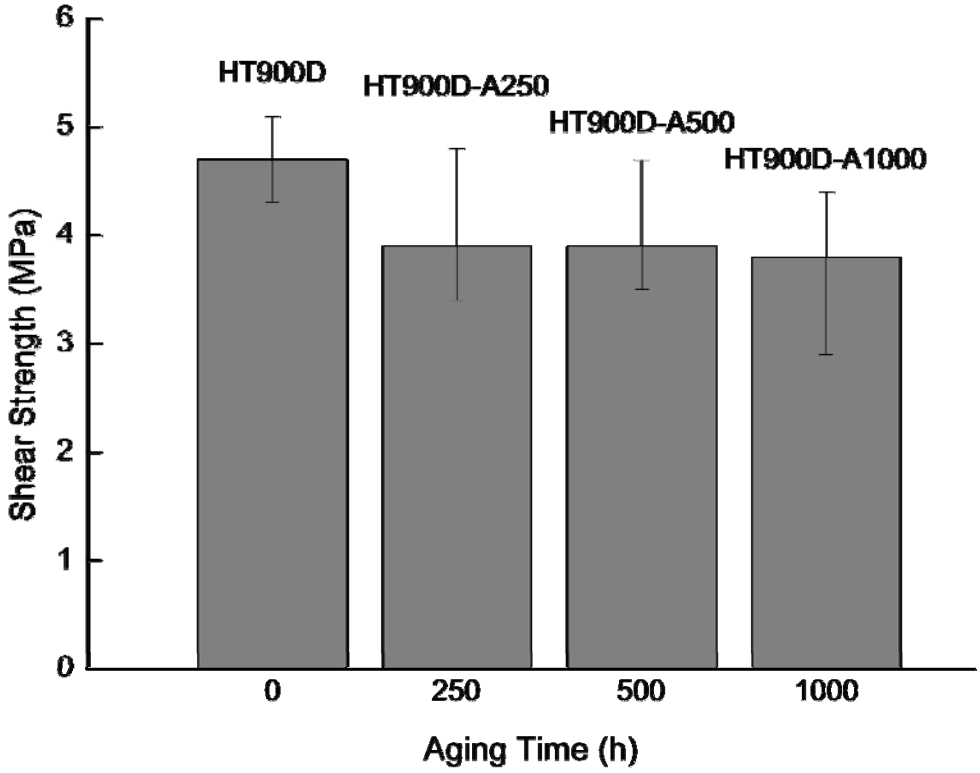

Fig. 35 Shear strength at 800 ^{o}C for specimens joined at 900 ^{o}C with various aging treatment times.

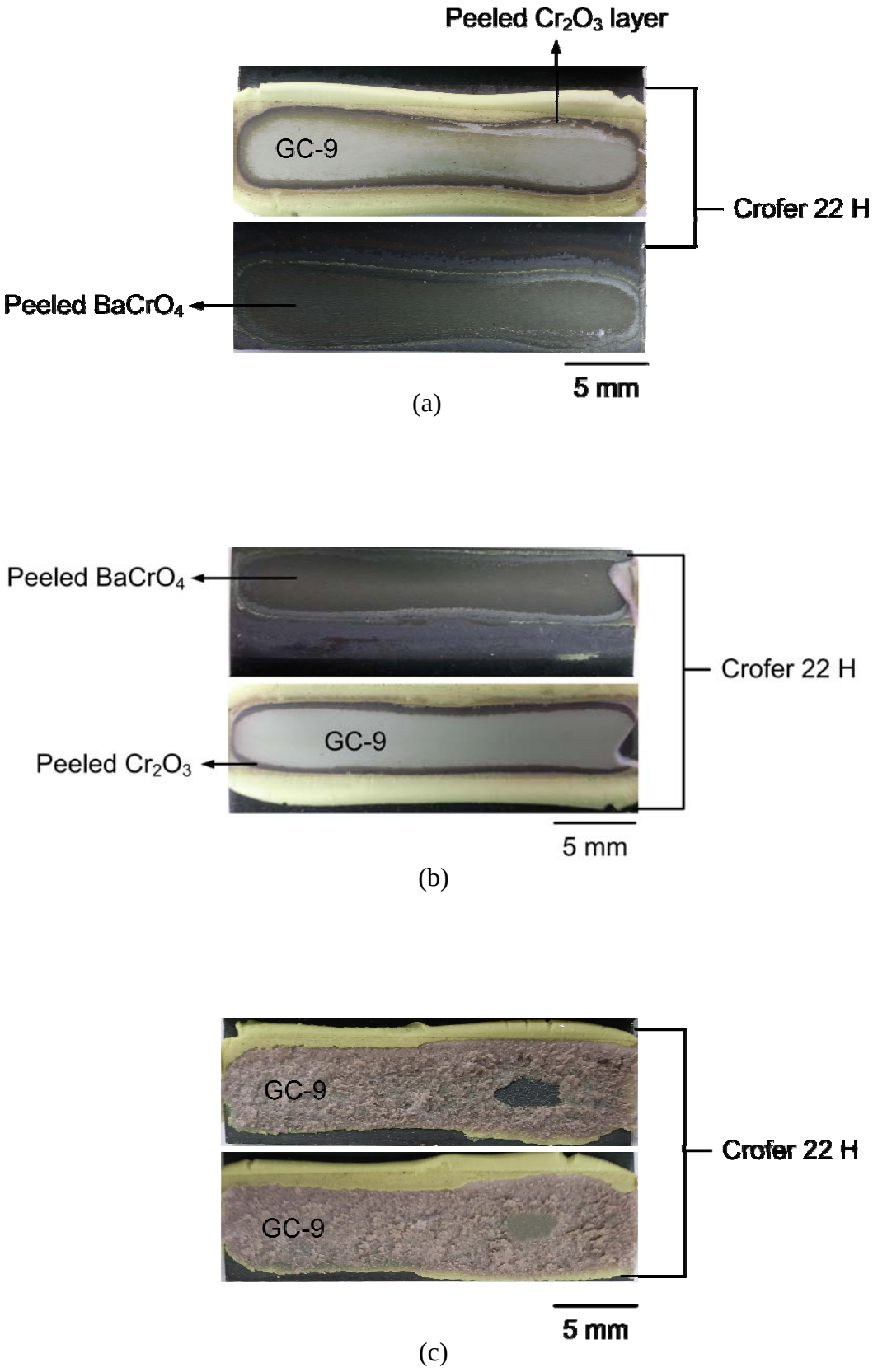

Fig. 36 Failure patterns of aged shear specimens tested at 800 ^{o}C: (a) HT900D-A250; (b) HT900D-A500; (c) HT900D-A1000.

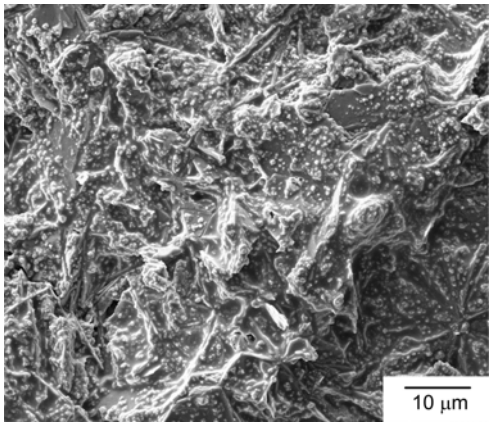

(a)

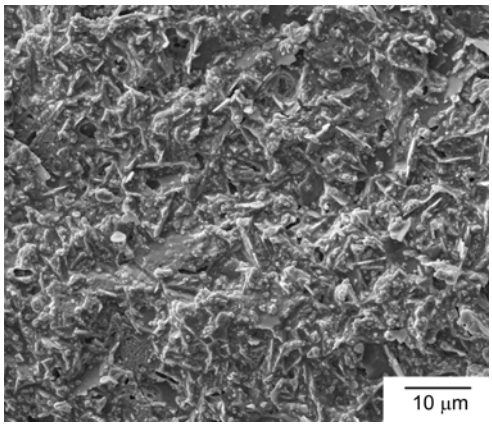

(b)

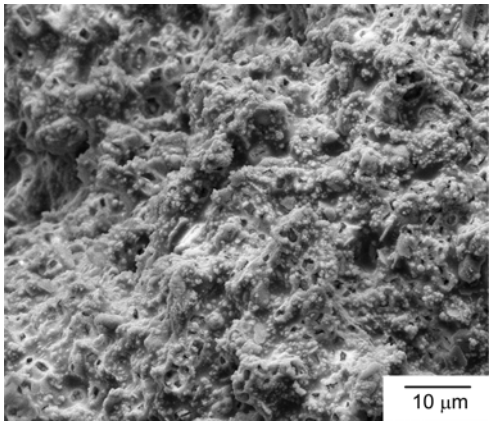

(c)

Fig. 37 SEM micrographs of fracture surface on the glass-ceramic layer in the shear specimens tested at 800 ^{o}C: (a) unaged HT900D; (b) aged HT900D-A500; (c) aged HT900D-A1000.

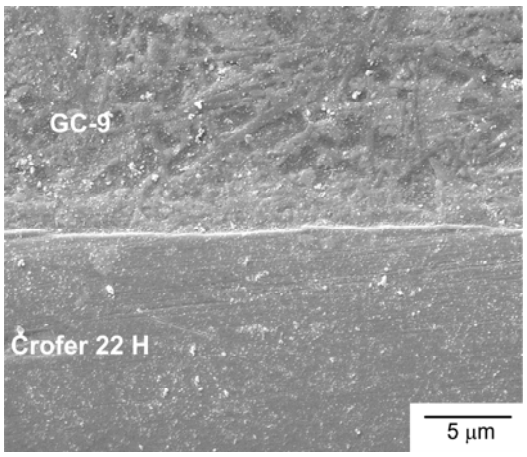

(a)

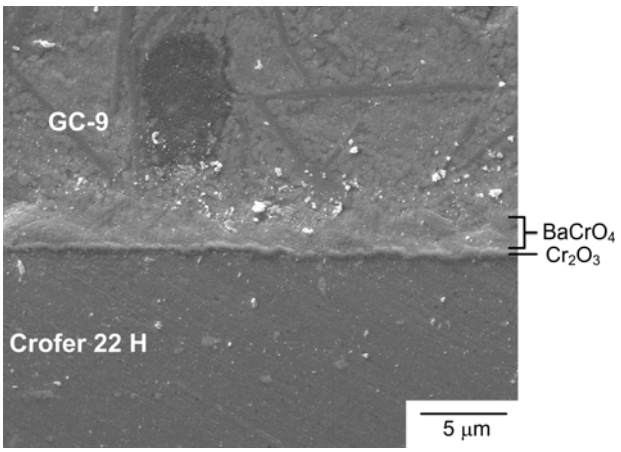

(b)

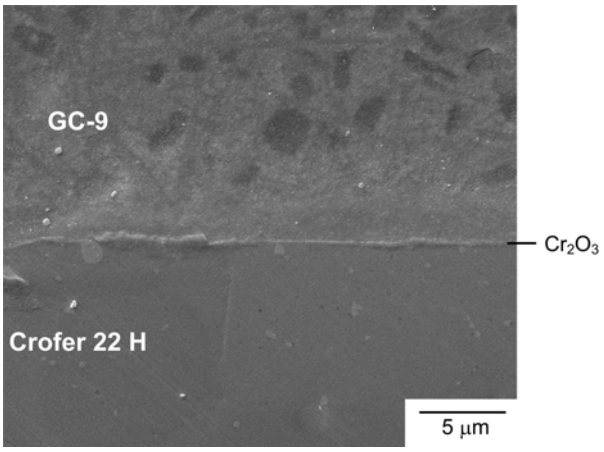

(c)

Fig. 38 SEM micrographs of a cross section of the interface between the GC-9 and Crofer 22 H in variously aged joint specimens: (a) HT900D-A250; (b) HT900D-A500; (c) HT900D-A1000.

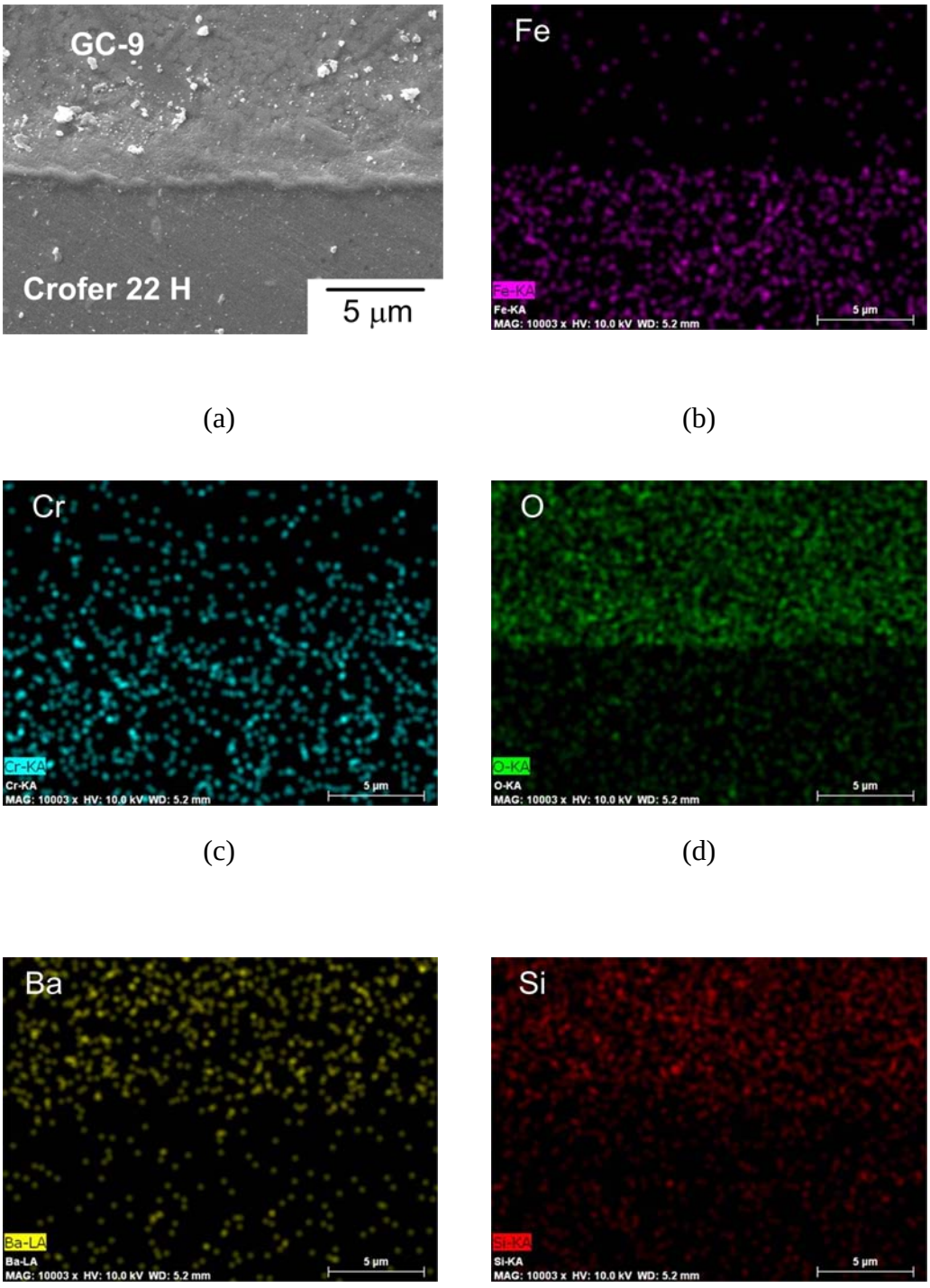

Fig. 39 EDS mapping of elements at the interface between GC-9 and Crofer 22 H in a joint specimen of HT900-A1000: (a) mapping region; (b) Fe; (c) Cr; (d) O; (e) Ba; (f) Si.

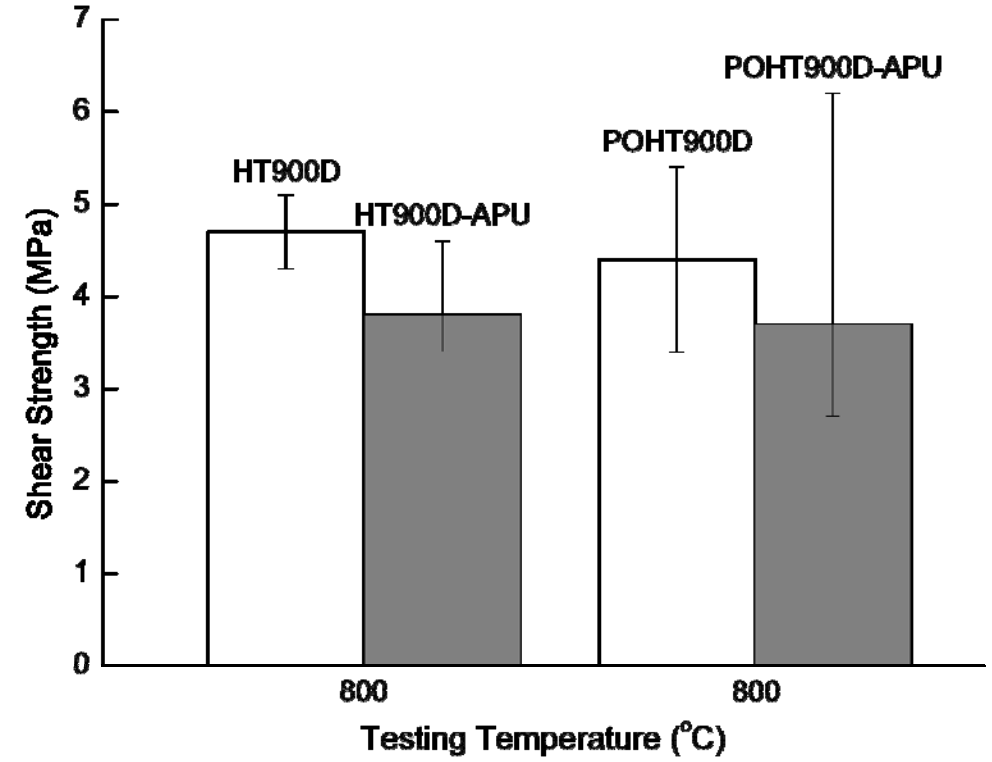

(a)

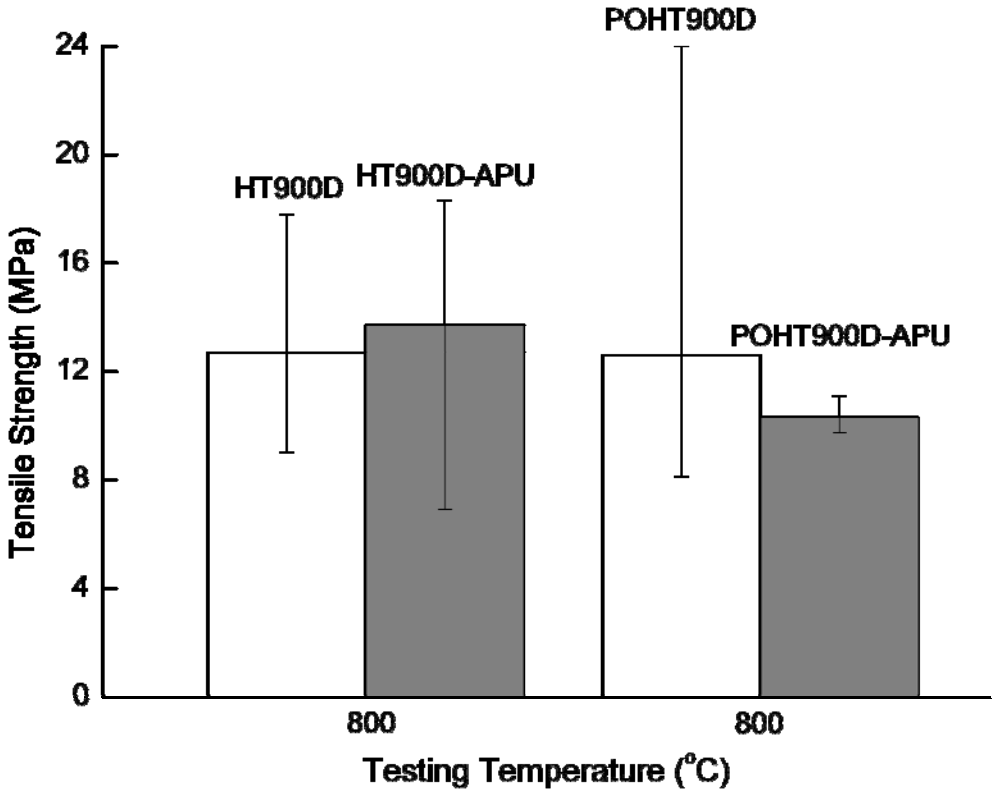

(b)

Fig. 40 Comparison of the (a) shear and (b) tensile strength of Crofer 22 H and APU joint specimens tested at 800 °C.

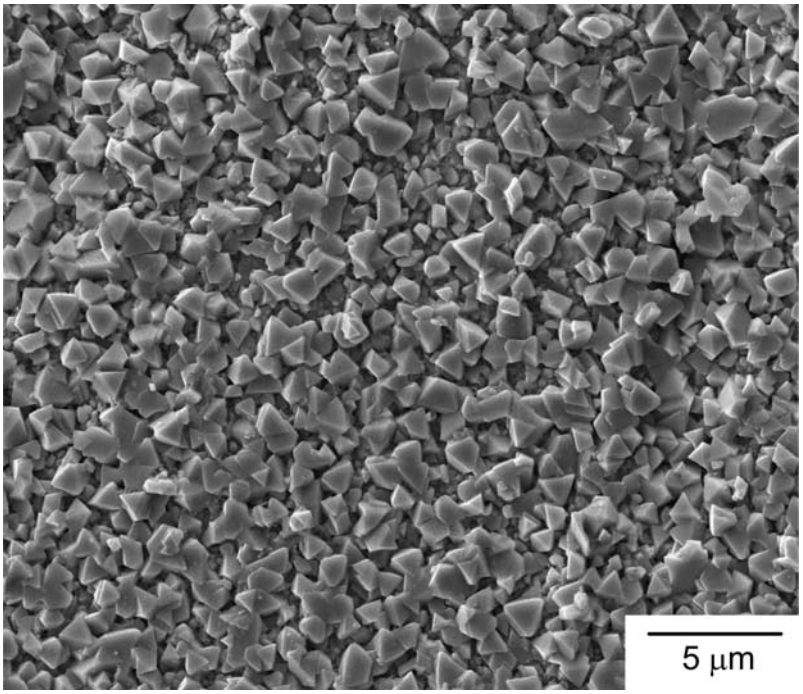

(a)

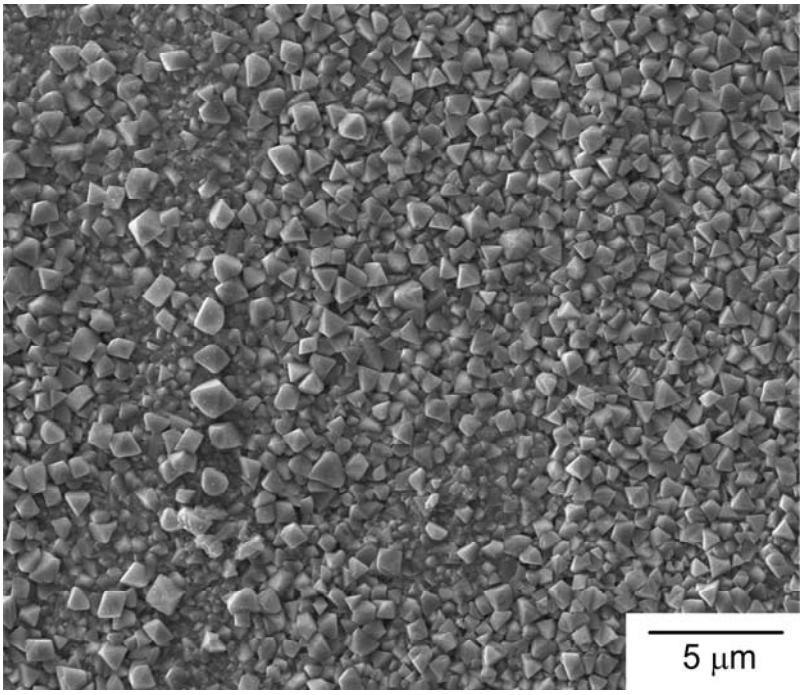

(b)

Fig. 41 SEM micrographs of the oxide scale on metallic interconnect after test: (a) Crofer 22 H; (b) Crofer 22 APU.

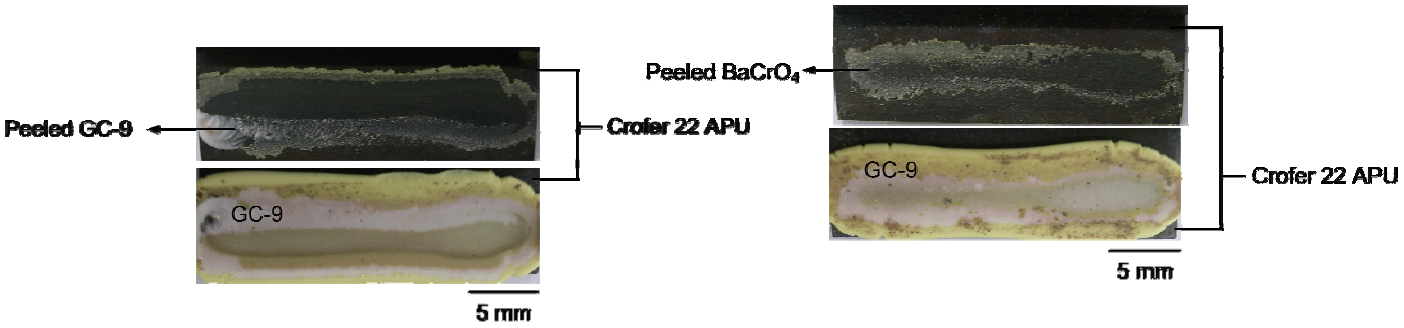

(a) (b)

Fig. 42 Failure patterns of shear specimens tested at 800 ^{o}C: (a) HT900D-APU; (b) POHT900D-APU.

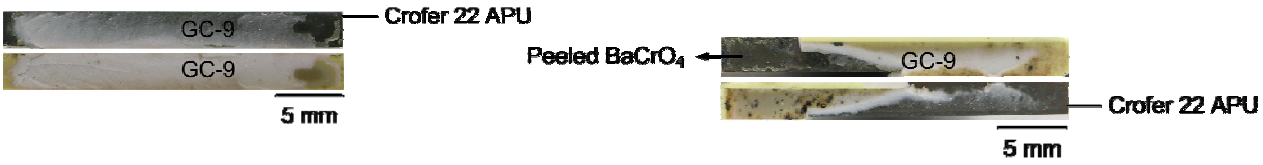

(a) (b)

Fig. 43 Failure patterns of tensile specimens tested at 800 ^{o}C: (a) HT900D-APU; (b) POHT900D-APU.

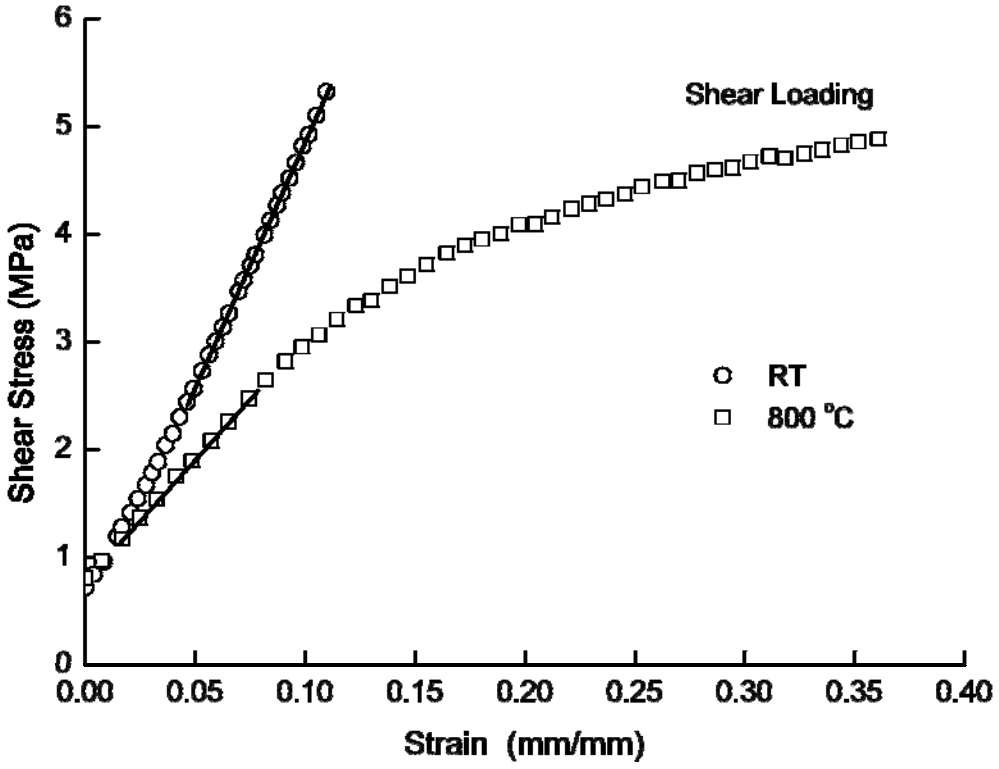

(a)

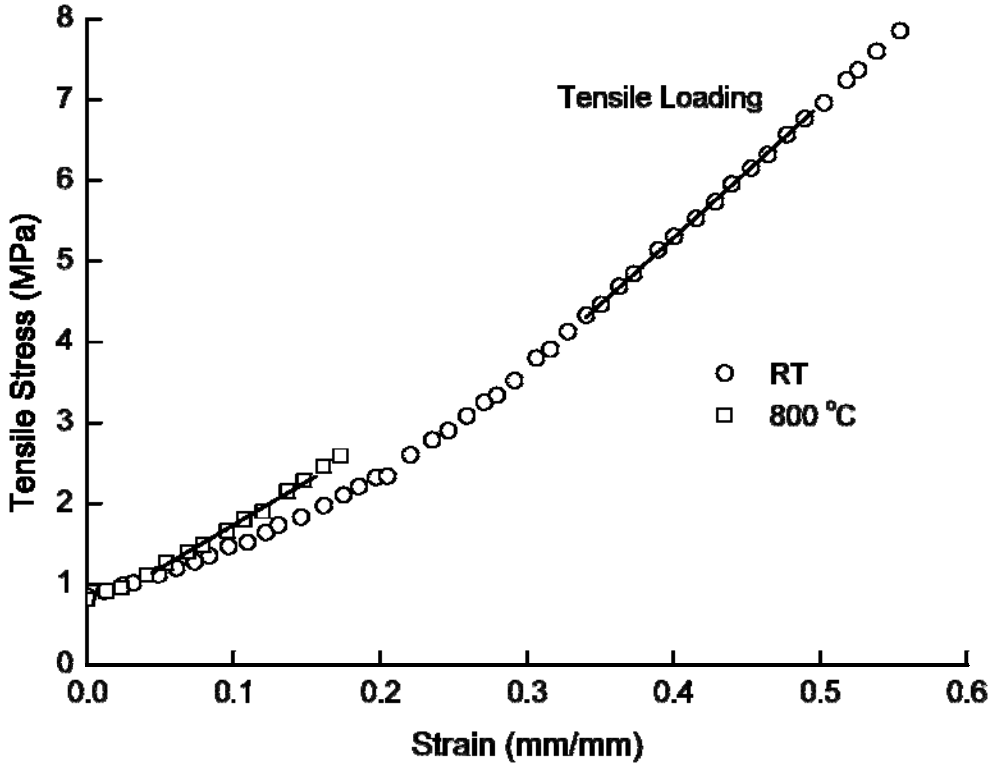

(b)

Fig. 44 Typical stress-strain curves of the joint specimens tested at RT and 800 ^{o}C under (a) shear and (b) tensile loading.